Desalination and Water Treatment
www.deswater.com

doi: 10.5004/dwt.2023.29770

301 (2023) 256–276
July

Method of evaluation of the transport properties in polymeric membrane systems using the N^r hybrid form of Kedem–Katchalsky–Peusner formalism

Andrzej Ślęzak[a], Izabella Ślęzak-Prochazka[b,c], Sławomir M. Grzegorczyn[d], Kornelia Batko[e], Wioletta M. Bajdur[f], Maria Włodarczyk-Makuła[g,*]

[a]*Collegium Medicum, Jan Dlugosz University, Częstochowa, Poland, email: aslezak52@gmail.com*
[b]*Department of Systems Biology and Engineering, Silesian University of Technology, Gliwice, Poland*
[c]*Biotechnology Centre, Silesian University of Technology, Gliwice, Poland, email: izabella.slezak-prochazka@polsl.pl*
[d]*Department of Biophysics, Faculty of Medical Science in Zabrze, Medical University of Silesia, Zabrze, Poland, email: grzegorczyn@sum.edu.pl*
[e]*Institute of Political Science, University of Silesia, Katowice, Poland, email: kornelia.batko@us.edu.pl*
[f]*Department of Innovation and Safety Management Systems, Częstochowa University of Technology, Częstochowa, Poland, email: wiolawb@poczta.onet.pl*
[g]*Faculty of Infrastructure and Environment, Częstochowa University of Technology, Częstochowa, Poland; email: m.wlodarczyk-makula@pcz.pl/mwm@is.pcz.czest.pl*

Received 30 May 2023; Accepted 12 July 2023

ABSTRACT

In this paper, the N^r hybrid version of the Kedem–Katchalsky–Peusner (K-K-P) formalism for concentration polarization conditions is developed. For ternary non-electrolyte solutions, this formalism includes the hybrid Peusner coefficients (N^r_{ij}, $i, j \in \{1, 2, 3\}$, r = A, B), which determine the transport properties of the membrane, the n^r_{ij} coefficients which determine the degree of coupling, and the energy conversion efficiency coefficient (e^r_{ij}). Besides, K-K-P formalism is the basis for a method to evaluate the conversion of internal energy (U-energy) into free energy (F-energy) and dissipated energy (S-energy) in a membrane system containing ternary non-electrolyte solutions separated by a polymer membrane. Moreover, it is shown that the Peusner coefficients are proposed as a flux-induced version of the modified Péclet number for concentration polarization conditions. The present paper is a continuation of several previous papers, of which the L^r, R^r, H^r, K^r versions of the Kedem–Katchalsky–Peusner formalism are presented. The formalism using the N^r form of the hybrid Kedem–Katchalsky–Peusner equations can be a useful tool to study the transport properties of artificial membranes for environmental engineering.

Keywords: Membrane transport; Concentration polarization; Peusner's network thermodynamics; N^r hybrid form of the Kedem–Katchalsky–Peusner equations; Entropy; Péclet number

1. Introduction

Energy conversion and transports of mass, energy and information are among the many phenomena that ensure the continuity of life under Earth's gravity. These phenomena occur in various types of nano-, micro- and macrosystems, including artificial membrane systems (e.g., water treatment systems, microcapsules containing drugs or in hemodialyzers) and biological cells. The study of membrane transport and energy conversion processes is both cognitive and applied in science, in various disciplines of technology, bioenergetics and biomedicine [1–3]. Cognitive research aims to understand the molecular mechanisms of fluid and solute exchange through biological and/or synthetic

* Corresponding author.

Presented at the 15th Scientific Conference on Micropollutants in the Human Environment, 14–16 September 2022, Częstochowa, Poland

membranes [4]. In living systems, membranes act, among other things, as regulators of mass and energy transport ensuring the maintenance of metabolic activity, pressure balance or structural integrity. Moreover, knowledge of membrane transport mechanisms plays an important role in water technology and wastewater technology, the food industry, biorefineries and renewable energy [5], and in medicine for drug carriers such as liposomes, nanomicelles or dendrimers [6] or active membrane dressings [7].

Many materials are used as membrane-forming materials. The first material developed in the 1960s for seawater desalination by reverse osmosis was cellulose acetate. Today, membrane separation processes are performed by reverse osmosis and ultrafiltration. They cover a wide range of technological activities such as seawater desalination, wastewater treatment, food processing or medical and biotechnological applications [8,9]. Currently, the most popular option due to its stability over wide pH ranges, higher temperatures and harsh chemical conditions is the thin-film polyamide composite membrane [10,11]. With a view to increasing the efficiency of membrane separation processes, the current trend in polymer-based membrane research is the development of nanocomposite membranes that use nanofillers such as single-walled carbon nanotubes, multi-walled carbon nanotubes, graphene, graphene oxide, silica or zeolite. The performance of membrane separation processes depends on many factors including the membrane structure and the size, shape and number of pores. The optimal membrane performance can be predicted from the average pore size and pore size distribution that characterize a given membrane surface [8].

All processes in physical and chemical systems, including living systems, require the supply of mass and energy. In living systems, the supply of mass and energy is carried out through the intake of specific nutrients, in which chemical potential energy, which is one of the form of solar energy, is stored. The direction of isothermal-isochoric processes is determined by free energy (*F*-energy), and isothermal-isobaric processes by free enthalpy (*G*-energy). *F*-energy is part of the internal energy (*U*-energy). These two energies are related to each other by the expression $dF = dU - TdS$, in which T is the absolute temperature and S is the thermodynamic entropy. In turn, the direction of isothermal-isobaric processes is determined by the free enthalpy (*G*-energy), which is a component of enthalpy (*H*-energy). Its part called free enthalpy (*G*) satisfies the equation $dG = dH - TdS$. The product of TdS is a measure of degraded energy (*S*-energy) [12,13].

In physical and chemical systems, including biological systems, *F*-energy and/or *G*-energy are converted into various types of work. The transformations of energy into useful work can occur by thermal, osmotic–diffusion, electrical and/or mechanical forms. They are determined by corresponding gradients (thermodynamic forces) of: temperature (*T*), concentration (*C*), electrical potentials (*V*) and/or mechanical pressure (*P*). A specific thermodynamic stimulus can induce specific transports: diffusive and/or osmotic transports of substances, heat, electrical charges, etc. [12,13].

The following models are used to describe transport processes in membrane systems: diffusion [14,15], frictional [16–18], statistical [19,20] models based on non-equilibrium Onsager thermodynamics [4,12,21] and network thermodynamics [22–35]. Derivation of membrane transport models within the framework of Onsager thermodynamics is based on the following procedure: (i) find the dissipation function, (ii) transform the dissipation function to account for the relevant thermodynamic forces and flows, and (iii) use practical forces and flows to give macroscopic phenomenological equations [4,12]. In the systems close to equilibrium, that is, those in which the rate of energy dispersion is small, the linearity of the relationship between fluxes and driving thermodynamic forces can be assumed. The Kedem–Katchalsky (KK) model, developed in accordance with these principles, takes into account the interaction between the solvent and solutes and is characterized by appropriate sets of phenomenological membrane coefficients (e.g., L_p, σ, ω), which can be determined experimentally independently [12]. Therefore, the KK equations belong to the group of basic research tools for membrane transport in both biological and artificial systems. Several versions of these equations are used: classical Kondepudi and Prigogine [13], Cheng and Pinsky [21], and Kedem, Katchalsky and Peusner [22–35], Kargol's [36], Elmoazzen et al. [37].

The first attempts to formulate the principles of network thermodynamics (NT) appeared in the work of Meixner [38], who was the first to note the relationship between irreversible transport systems and electrical networks. The idea of NT was developed by Peusner [22] in his Doctoral Thesis (1970), using non-equilibrium thermodynamics, symbolism and analog theory of electric circuits (Kirchhoff's current and voltage laws, Tellegen's principle, etc.) [28]. A year later, the work of Oster et al. [23] was published, which applied the bond graph method in NT to describe membrane transport. Peusner applied his ideas to energy conversion systems [24], membrane systems and processes [24], Brownian motions [26] and chemical reactions with diffusion [27]. He also proposed a method for hybrid transformation of linear Onsager equations [24,25,28] and showed ways to derive *L*, *R*, *H* and *P* versions of the Kedem–Katchalsky–Peusner (K-K-P) equations for homogeneous solutions by means of series of network transformations, and introduced the "super *Q*" coupling parameter. The *L* and *R* versions of the K-K-P equations contain symmetric Peusner coefficients L_{ij} and R_{ij}, respectively. In turn, the *H* and *P* versions contain asymmetric (hybrid) Peusner coefficients H_{ij} and P_{ij}. In addition, he demonstrated the relationship between geometric and network formulations of Onsager's principle using the concept of differential geometry metrics [28–30]. The Peusner's idea of NT (Peusner Network Thermodynamics, PNT) was developed by Ślęzak et al. for concentration polarizations conditions of binary [31–34] and ternary [35,39–41] non-electrolyte solutions separated by polymeric membrane. For binary solutions, we have four versions of the equations K-K-P: L^r, R^r, H^r and P^r. The L^r and R^r, versions of the K-K-P equations contain symmetric Peusner coefficients L^r_{ij} and R^r_{ij} ($i, j \in \{1, 2\}$, r = A, B), respectively. In turn, the H^r and P^r versions – asymmetric (hybrid) Peusner coefficients H^r_{ij} and P^r_{ij} ($i, j \in \{1, 2\}$, r = A, B). In turn, for ternary solutions, we have eight versions of the equations K-K-P: L^r, R^r, H^r, K^r, N^r, S^r, W^r and P^r. The L^r and R^r, versions of the K-K-P equations contain symmetric Peusner coefficients L^r_{ij}

and R^r_{ij} (i, j ∈ {1, 2, 3}, r = A, B). In turn, the H^r, K^r, N^r, S^r, W^r and P^r versions – hybrid Peusner coefficients L^r_{ij}, R^r_{ij}, H^r_{ij}, K^r_{ij}, N^r_{ij}, S^r_{ij}, W^r_{ij} and P^r_{ij} (i, j ∈ {1, 2, 3}, r = A, B). Versions of L^r, R^r, H^r and K^r of K-K-P equations have been used in previous papers [35–37,41]. The hybrid description developed by Peusner provides a more elegant physical interpretation of membrane transport processes than that implied by the Kedem–Katchalsky equations [20]. The present paper is a continuation of previous papers [35,39–41] in which the L^r, R^r, H^r and K^r versions of the Kedem–Katchalsky–Peusner formalism were presented.

This paper presents another hybrid version of the Kedem–Katchalsky–Peusner (K-K-P) formalism for ternary non-electrolyte solutions, which is denoted by N^r. This formalism includes the Peusner coefficients N^r_{ij}, N^r_{det} (i, j ∈ {1, 2, 3}, r = A, B), and defining the transport properties of the membrane. On their basis, the energy conversion efficiency coefficient (e^r_{ij}) and the degree of coupling between the transport processes (n^r_{ij}) were calculated. To evaluate of F-energy, we propose a new N^r form of the K-K-P equations, which include the Peusner coefficients N^r_{ij} (i, j ∈ {1, 2, 3}, r = A, B) and an equation for the global source of S-energy ($\left(\varphi^r_S\right)_{N^r}$). The coefficients N^r_{ij} and N_{ij}, matrix coefficients N^r_{det} = det[N^r] and N_{det} = det[N] can be calculated using the experimentally determined coefficients L_p, σ and w. To determine $\left(\varphi^r_S\right)_{N^r}$, we use the experimentally determined volume (J^r_v), glucose (J^r_{s1}) and/or ethanol (J^r_{s2}) fluxes. We calculate $\left(\varphi^r_S\right)_{N^r}$ for concentration polarization conditions of solution. In addition, we introduce the energy conversion efficiency coefficient $\left(e^r_{ij}\right)_{N^r}$, which is necessary to determine the F-energy. The results presented here improve our understanding of membrane transport under concentration polarization conditions. In this paper, a cellulose membrane (Nephrophan) was used. But our method for determining F-energy can be adapted to other types of membranes and membranous processes. It can also be used to understand the molecular mechanisms of membrane transport in order to improve the energy properties of new membrane systems. In turn on the basis of $(e^r_{ij})_R$ and $(\Phi^r_S)_R$ the flux of free energy (F-energy) ($(\Phi^r_F)_R$) and the flux of internal energy (U-energy) ($(\Phi^r_U)_R$) were calculated. The relationship between Peusner coefficients and the modified Péclet number were also demonstrated.

2. Materials and methods

2.1. Membrane system

Similarly to previously published papers [35,39–41], membrane transport was studied in a system containing two non-electrolyte ternary solutions separated by a polymer membrane, shown schematically in Fig. 1a. In this system, the membrane (M) separating compartments (h) and (l) is isotropic, symmetric, electrically inert and selective for solvent and solutes. The concentrations of solutes filling compartments (h) and (l) at the initial moment (t = 0) are defined as C_{hk} and C_{lk} ($C_{hk} > C_{lk}$, k = 1, 2). For a horizontally oriented membrane (perpendicular to the gravity vector), the solutions were set in configurations A or B (r = A or B). In configuration A, the solution with a concentration C_{lk} was placed in the compartment above the membrane, while the solution with a concentration C_{hk} was placed in the compartment below the membrane. In configuration B, the locations of the solutions relative to the membrane were reversed.

We have investigated isothermal and stationary transport processes trough the membrane, characterized by volume (J^r_v) and solute fluxes (J^r_{sk}) (k = 1, 2 and r = A, B). These fluxes can be described for ternary non-electrolyte solutions and concentration polarization conditions by means of the KK equations [31–35,39–41]. As is known [42–48], solute molecules diffusing through the membrane under concentration polarization conditions form concentration boundary layers (CBLs) on both sides of the membrane. These CBLs are denoted by l^r_h and l^r_l and their thicknesses by δ^r_h and δ^r_l, respectively [44,45]. Creation of l^r_h and l^r_l results in a decrease

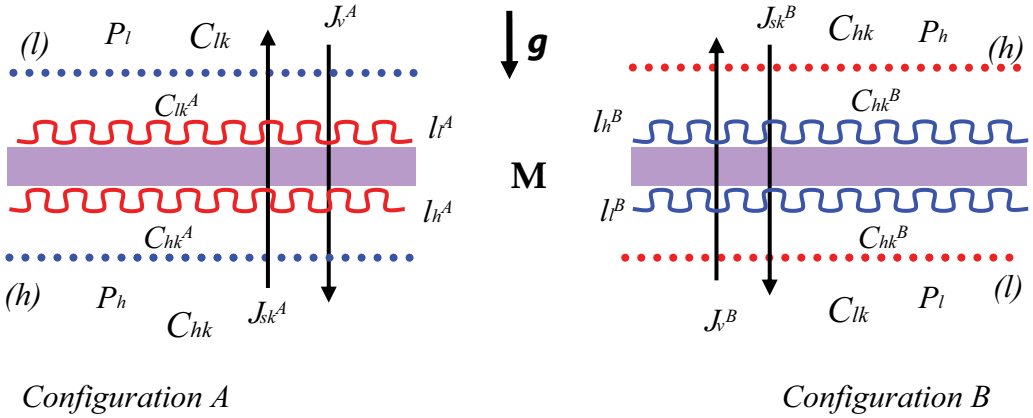

Fig. 1. Model of single-membrane system: M – membrane, g – gravitational acceleration, $l^A_l$and l^A_h – the concentration boundary layers in configuration A, $l^B_l$and l^B_h – the concentration boundary layers in configuration B, (the blue and red dotted lines refer to the stable state of l^r_l and l^r_h, r = A or B, while the red and blue broken lines refer to the unstable state of l^r_l and l^r_h, r = A or B), P_h and P_l – mechanical pressures, C_{kh} and C_{kl} – global solutes concentrations ($C_{hk} > C_{lk}$), C^A_{lk}, C^A_{hk}, C^B_{lk} and C^B_{hk} – local (at boundaries between membrane and CBLs) solutes concentrations, J^A_{sk} and J^A_v – solute and volume fluxes in configuration A, J^B_{sk} and J^B_v – solute and volume fluxes in configuration B, (k = 1 or 2).

of solute concentration at the membrane-solution interface from C_{hk} to C^r_{hk} and an increase from C_{lk} to C^r_{lk}. This means that for $t > 0$ the following relationships are satisfied: $C^r_{hk} > C^r_{hk}$, $C^r_{lk} > C_{lk}$ and $C_{hk} > C^r_{hk}$ (k = 1, 2) [33]. The solution densities denoted by the symbols ρ^r_l and ρ^r_h refer to the densities of the solutions at the boundary of the layers l^r_l/M and M/l^r_h as well as ρ_l and ρ_h refer to the densities of the solutions outside the layers. The following relationships are possible between suitable solutions densities: $\rho_l < \rho_h$ or $\rho_l > \rho_h$, $\rho^r_l > \rho_l$ or $\rho^r_l < \rho^r_h$, $\rho^r_l > \rho^r_h$ or $\rho^r_l < \rho^r_h$ and $\rho^r_h > \rho_h$ or $\rho^r_h < \rho_h$. The relations between densities and concentrations of solutions can be described by $\rho_h = \rho_l(1 + \alpha_1 C_{h1} + \alpha_2 C_{h2})$, where $\alpha_1 = \rho_l^{-1}\partial\rho/\partial C_1$ and $\alpha_2 = \rho_l^{-1}\partial\rho/\partial C_2$ (for glucose in aqueous ethanol solutions $\alpha_1 > 0$ and $\alpha_2 < 0$) [43]. If the solution with lower density is in the compartment above the membrane, the l^r_h/M/l^r_l complex is hydrodynamically stable. If, on the other hand, the solution with lower density is in the compartment below the membrane, the l^r_h/M/l^r_l complex may lose hydrodynamic stability and gravitational (convective) instabilities appear near the membrane [38,42,43]. The tests were performed for a situation in which compartments (*h*) and (*l*) contained solutions of glucose (index 1) in an aqueous ethanol solution (index 2) of different concentrations. The solutions were separated by a Nephrophan membrane (Orwo VEB Filmfabrik, Wolfen, Germany) made of cellulose acetate, with hydrophilic pores (averaged pore diameter of 2.4 nm and total thickness of 14–15 μm) [49,50]. The electron microscope image of surface and cross-section of this membrane was presented in [43]. Nephrophan has been used as a hemodialyzer and ocular drug delivery system [49,51]. In this and our previous papers [18,31–35,39–48], the Nephrophan membrane was treated as a "black box" for solvent and solutes. Compartment (*l*) contained a solution in which the concentrations of both components were constant: $C_{l1} = C_{l2} = 1$ mol·m^{-3}. Compartment (*h*) contained glucose in an aqueous ethanol solution. The concentration of glucose was changed from 1 to 71 mol·m^{-3} and the concentration of ethanol was fixed at 201 mol·m^{-3}. This means that the osmotic pressure difference of the aqueous glucose solutions ($\Delta\pi_1$) was in the range of 0–171.6 kPa. The difference of osmotic pressure for ethanol ($\Delta\pi_2$) was constant and equal to 490.2 kPa. The transport properties of this membrane were determined by the following parameters: hydraulic permeability (L_p), reflectivity (σ) and diffusion permeability (ω) [8]. The values of these coefficients for glucose (index 1) and ethanol (index 2) for Nephrophan membrane are: $L_p = 4.9 \times 10^{-12}$ m^3·N^{-1}·s^{-1}, $\sigma_1 = 0.068$, $\sigma_2 = 0.025$, $\omega_{11} = 0.8 \times 10^{-9}$ mol·N^{-1}·s^{-1}, $\omega_{12} = 0.81 \times 10^{-13}$ mol·N^{-1}·s^{-1}, $\omega_{22} = 2.0 \times 10^{-9}$ mol·N^{-1}·s^{-1} and $\omega_{21} = 1.63 \times 10^{-12}$ mol·N^{-1}·s^{-1} [46]. Besides, experimentally measured $\alpha_1 = 6.0 \times 10^{-5}$ kg·mol^{-1} and $\alpha_1 = -0.90 \times 10^{-5}$ kg·mol^{-1} were also used. A measure of concentration polarization are the concentration polarization coefficients (ζ^r_v, ζ^r_k, k = 1, 2; r = A, B), which for ternary solutions depend on both the concentration and composition of the solutions separated by the membrane and the configuration of the membrane system. The values of these coefficients were determined in previous paper [41] for Nephrophan membrane and glucose solutions in aqueous ethanol solution and are summarized in Table 1.

Table 1
Values of concentration polarization coefficients (ζ^r_v, ζ^r_k, k = 1, 2; r = A, B), for Nephrophan membrane and glucose in aqueous ethanol solution [41]

Δπ (kPa)	ζ^A_v	ζ^A_1	ζ^A_2	Δπ (kPa)	ζ^B_v	ζ^B_1	ζ^B_2
–171.57	0.031	0.028	0.03	6.13	0.031	0.028	0.029
–159.31	0.031	0.028	0.03	12.25	0.031	0.028	0.028
–147.06	0.031	0.028	0.03	24.51	0.031	0.028	0.029
–134.05	0.032	0.028	0.03	36.76	0.031	0.028	0.028
–122.55	0.037	0.028	0.032	49.02	0.041	0.028	0.03
–110.29	0.067	0.058	0.06	61.27	0.055	0.038	0.048
–98.04	0.15	0.18	0.16	73.53	0.095	0.062	0.082
–85.78	0.42	0.3	0.31	85.78	0.16	0.163	0.163
–73.53	0.29	0.44	0.44	98.04	0.295	0.306	0.304
–61.27	0.47	0.46	0.45	110.29	0.38	0.405	0.4
–49.02	0.49	0.48	0.487	122.55	0.435	0.45	0.44
–36. 76	0.495	0.485	0.487	134.05	0.468	0.475	0.47
–24.51	0.5	0.497	0.491	147.06	0.485	0.49	0.48
–12.25	0.5	0.497	0.492	159.31	0.496	0.496	0.496
–6.13	0.5	0.497	0.495	171.57	0.5	0.5	0.5

2.2. N^r form of Kedem–Katchalsky–Peusner equations for non-electrolyte solutions

As is known [42–46], the creation of concentration boundary layers (CBLs) occurs on both sides of a membrane separating two solutions of different concentration and/or composition. The process of CBLs creation is called concentration polarization. Concentration polarization leads to a reduction in membrane transport, involving a decrease in volume and solute fluxes from J_v and J_{sk} (for homogeneous solution) to J^r_v and J^r_{sk}, respectively (under conditions of concentration polarization). The fluxes J^r_v and J^r_{sk} depend on the configuration of the membrane system, and the concentration characteristics of J^r_v and J^r_{sk} for ternary solutions are nonlinear [41,46]. These fluxes can be described by the Kedem–Katchalsky equations for ternary non-electrolyte solutions, and the concentration polarization conditions can be described by the equations:

$$J^r_v = \zeta^r_p L_p \Delta P - \zeta^r_p L_p \left(\zeta^r_{v1}\sigma_{v1}\Delta\pi_1 + \zeta^r_{v2}\sigma_{v2}\Delta\pi_2\right) \quad (1)$$

$$J^r_{s1} = \zeta^r_{s11}\omega_{11}\Delta\pi_1 + \zeta^r_{s12}\omega_{12}\Delta\pi_2 + \bar{C}_1\left(1 - \zeta^r_{a1}\sigma_{a1}\right)J^r_v \quad (2)$$

$$J^r_{s2} = \zeta^r_{s21}\omega_{21}\Delta\pi_1 + \zeta^r_{s22}\omega_{22}\Delta\pi_2 + \bar{C}_2\left(1 - \zeta^r_{a2}\sigma_{a2}\right)J^r_v \quad (3)$$

where J^r_v – volume flux, J^r_{s1} and J^r_{s2} – fluxes of dissolved substances "1" and "2", respectively, L_p – hydraulic permeability coefficient, σ_{v1} and σ_{v2} – membrane reflection coefficients for substances "1" and "2" and volume flux, σ_{s1} and σ_{s2} – membrane reflection coefficients for substances "1" and "2" and solute flux, σ_{a1} and σ_{a2} – membrane reflection coefficients for substances "1" and "2" and advective flux, ω_{11} and ω_{22} – membrane permeability coefficients for substances "1" and "2" generated by osmotic pressure with indexes "1" and "2", respectively, and ω_{12} and ω_{21} – solute permeability coefficients for substances "1" and "2" generated by osmotic pressures with the indices "2" and "1", respectively,

ζ_p^r – hydraulic concentration polarization coefficient, ζ_{v1}^r and ζ_{v2}^r – osmotic concentration polarization coefficients, ζ_{s11}^r, ζ_{s12}^r, ζ_{s21}^r and ζ_{s22}^r – coefficients of diffusive concentration polarization and ζ_{a1}^r and ζ_{a2}^r – coefficients of advective concentration polarization. $\Delta P = P_h - P_l$ is the difference of hydrostatic pressures on the membrane (P_h and P_l means higher and lower hydrostatic pressure value). $\Delta\pi_k = RT(C_{kh} - C_{kl})$ is the difference of osmotic pressures on the membrane (RT is the product of the gas constant and the absolute temperature, while C_{kh} and C_{kl} are the concentrations of the solutions, $C_{hk} > C_{lk}$, $k = 1, 2$. $\bar{C}_k = (C_{hk} - C_{lk})[\ln(C_{hk}C_{lk}^{-1})]^{-1}$ ($k = 1, 2$) is the average concentration of solutes in the complex l_l^r/M/l_h^r, l_l^r and l_h^r – concentration boundary layers, M – membrane. For $\Delta\pi_k = 0 (C_{kh} = C_{kl})$ the Eqs. (1)–(3) take the form: $J_v^r = \zeta_p^r L_p \Delta P$, $J_{s1}^r = \bar{C}_1 (1 - \zeta_{a1}^r \sigma_{a1}) J_v^r$ and $J_{s2}^r = \bar{C}_2 (1 - \zeta_{a2}^r \sigma_{a2}) J_v^r$. After simple algebraic transformations we get $J_{ak}^r = \bar{C}_k (1 - \zeta_{ak}^r \sigma_{ak}) \zeta_p^r L_p \Delta P$, ($k = 1, 2$).

On the basis of Eqs. (1)–(3), the phenomenological coefficients for homogeneous solutions ($\zeta_p^r = \zeta_v^r = \zeta_s^r = \zeta_a^r = 1$) are defined as follows:

$$L_p = \left.\frac{J_v}{\Delta P}\right|_{\Delta C=0} \tag{4}$$

$$\sigma_{vk} = \left.\frac{\Delta P}{RT\Delta C}\right|_{J_{vk}=0,\ k=1 \text{ or } 2} \tag{5}$$

$$\sigma_{ak} = 1 - \left.\frac{J_{ak}}{\bar{c} L_p \Delta P}\right|_{\Delta C=0, C_{hk}=C_{lk},\ k=1 \text{ or } 2} \tag{6}$$

$$\omega_{sk} = \left.\frac{J_{sk}}{RT\Delta C}\right|_{J_v=0,\ s,k=1,2} \tag{7}$$

The set of membrane transport parameters (L_p, σ_{vk}, σ_{ak}, ω_{sk}) play the role of proportionality coefficients between thermodynamic forces and fluxes. The coefficients ζ_p^r, ζ_{vk}^r, ζ_s^r and ζ_{ak}^r play a similar role. The products $L_p\zeta_p^r$, $\sigma_{vk}\zeta_{vk}^r$, $\omega_{sk}\zeta_{sk}^r$ and $\sigma_{ak}\zeta_{ak}^r$, determine the transport properties of the complex: membrane and concentration boundary layers.

Using the principles of network thermodynamics, Eqs. (1)–(3) can be transformed to a hybrid form:

$$\Delta P - \Delta\pi_1 - \Delta\pi_2 = \frac{1}{L_p\zeta_p^r} J_v^r - \bar{C}_1\left(1 - \sigma_{v1}\zeta_{v1}^r\right)\frac{\Delta\pi_1}{\bar{C}_1} - \bar{C}_2\left(1 - \sigma_{v2}\zeta_{v2}^r\right)\frac{\Delta\pi_2}{\bar{C}_2} \tag{8}$$

$$\frac{\Delta\pi_1}{\bar{C}_1} = -\frac{\left(1 - \sigma_{a1}\zeta_{a1}^r\right)}{\omega_{11}\zeta_{s11}^r} J_v^r + \frac{1}{\bar{C}_1\omega_{11}\zeta_{s11}^r} J_1^r - \frac{\bar{C}_2\omega_{12}\zeta_{s12}^r}{\bar{C}_2\omega_{11}\zeta_{s11}^r}\frac{\Delta\pi_2}{\bar{C}_2} \tag{9}$$

$$J_2^r = \bar{C}_2\left(1 - \sigma_{a2}\zeta_{a2}^r\right) J_v^r + \bar{C}_1\omega_{21}\zeta_{s21}^r\frac{\Delta\pi_1}{\bar{C}_1} + \bar{C}_2\omega_{22}\zeta_{s22}^r\frac{\Delta\pi_2}{\bar{C}_2} \tag{10}$$

Using Eq. (9) in Eqs. (8) and (10), the N^r form of the Kedem–Katchalsky–Peusner equations are obtained can be presented as:

$$\Delta P - \Delta\pi_1 - \Delta\pi_2 = N_{11}^r J_v^r + N_{12}^r J_1^r + N_{13}^r\frac{\Delta\pi_2}{\bar{C}_2} \tag{11}$$

$$\frac{\Delta\pi_1}{\bar{C}_1} = N_{21}^r J_v^r + N_{22}^r J_1^r + N_{23}^r\frac{\Delta\pi_2}{\bar{C}_2} \tag{12}$$

$$J_2^r = N_{31}^r J_v^r + N_{32}^r J_1^r + N_{33}^r\frac{\Delta\pi_2}{\bar{C}_2} \tag{13}$$

where

$$N_{11}^r = \frac{1}{L_p\zeta_p^r} + \bar{C}_1\left[\frac{\left(1 - \sigma_{v1}\zeta_{v1}^r\right)}{\omega_{11}\zeta_{s11}^r}\frac{\left(1 - \sigma_{a1}\zeta_{a1}^r\right)}{\omega_{11}\zeta_{s11}^r}\right] \tag{14}$$

$$N_{12}^r = \frac{\left(1 - \sigma_{v1}\zeta_{v1}^r\right)}{\omega_{11}\zeta_{s11}^r} \tag{15}$$

$$N_{13}^r = \frac{\bar{C}_2\omega_{12}\zeta_{s12}^r\left(1 - \sigma_{v1}\zeta_{v1}^r\right)}{\omega_{11}\zeta_{s11}^r} - \frac{\bar{C}_2\omega_{11}\zeta_{s11}^r\left(1 - \sigma_{v2}\zeta_{v2}^r\right)}{\omega_{11}\zeta_{s11}^r} \tag{16}$$

$$N_{21}^r = -\frac{1 - \sigma_{a1}\zeta_{a1}^r}{\omega_{11}\zeta_{s11}^r} \tag{17}$$

$$N_{22}^r = \frac{1}{\bar{C}_1\omega_{11}\zeta_{s11}^r} \tag{18}$$

$$N_{23}^r = -\frac{\bar{C}_2\omega_{12}\zeta_{s12}^r}{\bar{C}_1\omega_{11}\zeta_{s11}^r} \tag{19}$$

$$N_{31}^r = \frac{\bar{C}_2\omega_{11}\zeta_{s11}^r\left(1 - \sigma_{a2}\zeta_{a2}^r\right)}{\omega_{11}\zeta_{s11}} - \frac{\bar{C}_1\omega_{21}\zeta_{s21}^r\left(1 - \sigma_{a1}\zeta_{a1}^r\right)}{\omega_{11}\zeta_{s11}} \tag{20}$$

$$N_{32}^r = \frac{\omega_{21}\zeta_{s21}^r}{\omega_{11}\zeta_{s11}^r} \tag{21}$$

$$N_{33}^r = \frac{\bar{C}_2[\omega_{11}\zeta_{s11}^r\omega_{22}\zeta_{s22} - \omega_{21}\zeta_{s21}^r\omega_{12}\zeta_{s12}^r}{\omega_{11}\zeta_{s11}} \tag{22}$$

Eqs. (11)–(22), represent the form of N^r Kedem–Katchalsky–Peusner equations. These equations can also be written in the matrix form:

$$\begin{bmatrix} \Delta P - \Delta\pi_1 - \Delta\pi_2 \\ \frac{\Delta\pi_1}{\bar{C}_1} \\ J_r^2 \end{bmatrix} = \begin{bmatrix} N_{11}^r & N_{12}^r & N_{13}^r \\ N_{21}^r & N_{22}^r & N_{23}^r \\ N_{31}^r & N_{32}^r & N_{33}^r \end{bmatrix} \begin{bmatrix} J_v^r \\ J_1^r \\ \frac{\Delta\pi_2}{\bar{C}_2} \end{bmatrix} = \left[N^r\right] \begin{bmatrix} J_v^r \\ J_1^r \\ \frac{\Delta\pi_2}{\bar{C}_2} \end{bmatrix} \tag{23}$$

where $[N^r]$ is a matrix of Peusner coefficients N_{ij}^r ($i, j \in \{1, 2, 3\}$) for ternary non-electrolyte solutions and concentration polarization conditions.

Eqs. (14)–(22) shows that for non-diagonal coefficients the relations $N^r_{12} \neq N^r_{21}$, $N^r_{13} \neq N^r_{31}$ and $N^r_{23} \neq N^r_{32}$ are satisfied. Moreover, it can be shown that the determinant of the matrix $[N^r]$ is equal to:

$$\det\left[N^r\right] = N^r_{\det} = \frac{\bar{C}_2\begin{bmatrix}\omega_{22}\zeta^r_{s2} + \bar{C}_2 L_p \zeta^r_p\left(1-\sigma_{a2}\zeta^r_{a2}\right)\\ \left(1-\sigma_{v2}\zeta^r_{v2}\right)\end{bmatrix}}{\bar{C}_1 L_p \zeta^r_p \omega_{11}\zeta_{s11}} \tag{24}$$

The superscript "*r*" in Eqs. (11)–(22) means that the fluxes J^r_v, J^r_1, J^r_2, the coefficients N^r_{ij} (i, $j \in \{1, 2, 3\}$; r = A, B) and the matrix $[N^r]$ of these coefficients, relating to concentration polarization conditions, are dependent on the configuration of the membrane system. For solution homogeneity conditions, the conditions $\zeta^r_{v1} = \zeta^r_{v2} = \zeta^r_{a1} = \zeta^r_{a2} = \zeta^r_{s11} = \zeta^r_{s12} = \zeta^r_{s22} = \zeta^r_{s21} = \zeta^r_p = 1$, $J^r_v = J_v$, $J^r_1 = J_1$, $J^r_2 = J_2$, and $N^r_{ij} = N_{ij}$ are fulfilled.

2.3. Mathematical model of energy conversion in the membrane system

In thermodynamic systems, also in membrane systems, the internal energy (*U*-energy) can be converted into free energy (*F*-energy) and the dissipated energy (*S*-energy) [4,12,13]. The fluxes of these quantities satisfy the following equation:

$$\left[\left(\phi^r_U\right)_{N^r}\right]_{ij} = \left[\left(\phi^r_F\right)_{N^r}\right]_{ij} + \left(\phi^r_S\right)_{N^r} \tag{25}$$

where $\left(\phi^r_U\right)_{N^r} = A^{-1}dU^r/dt$ is the flux of U-energy, $\left(\phi^r_F\right)_{N^r} = A^{-1}dF^r/dt$ is the flux of F-energy, $\left(\phi^r_F\right)_{N^r} = TA^{-1}d_iS^r/dt$ – is the flux of dissipated energy (S-energy), d_iS/dt – is the rate of entropy creation in the membrane system by irreversible processes (flux of cumulative entropy creation), T – absolute temperature, and A – the membrane surface area.

If the solutions contain a solvent and two dissolved substances, then the N^r version of dissipated energy for the concentration polarization conditions denoted by $\left(\varphi^r_S\right)_{N^r}$ is described by the equation.

$$\left(\phi^r_S\right)_{N^r} = \left(\phi^r_S\right)_{J^r_v} + \left(\phi^r_S\right)_{J^r_1} + \left(\phi^r_S\right)_{J^r_2} = J^r_v\left(\Delta P - \Delta\pi_1 - \Delta\pi_2\right) + J^r_{s1}\frac{\Delta\pi_1}{\bar{C}_1} + J^r_{s2}\frac{\Delta\pi_2}{\bar{C}_2} \tag{26}$$

where $\left(\varphi^r_S\right)_{N^r}$ is the N^r version of dissipated energy for the concentration polarization conditions, $\left(\phi^r_S\right)_{J^r_v}$ is the dissipated energy produced by J^r_v, $\left(\phi^r_S\right)_{J^r_{sk}}$ is the dissipated energy produced by J^r_{s1}, J^r_v and J^r_{s2} – the volume and solute fluxes, respectively, for the concentration polarization conditions of the solutions, r = A or B means the configuration of the membrane system, k = 1, 2).

Using Eqs. (11)–(13), Eq. (15) can be transformed to the form:

$$\left(\phi^r_S\right)_{N^r} = \alpha^r_1\left(J^r_v\right)^2 + \alpha^r_2 J^r_v J^r_{s1} + \alpha^r_3 J^r_v J^r_{s2} + \alpha^r_4\left(J^r_{s1}\right)^2 + \alpha^r_5 J^r_{s1} J^r_{s2} + \alpha^r_6\left(J^r_{s2}\right)^2 \tag{27}$$

where $\alpha^r_1 = N^r_{11}$, $\alpha^r_2 = N^r_{12} + N^r_{21} - N^r_{23}N^r_{31}N^{r\,-1}_{33}$, $\alpha^r_3 = N^r_{13} - N^r_{31}N^{r\,-1}_{33}$, $\alpha^r_4 = N^r_{22} - N^r_{23}N^r_{32}N^{r\,-1}_{33}$, $\alpha^r_5 = (N^r_{23} - N^r_{32})N^{r\,-1}_{33}$, $\alpha^r_6 = N^{r\,-1}_{33}$.

Eq. (27) shows the N^r version of the *S*-energy dissipation for the concentration polarization conditions. The $\left(\varphi^r_S\right)_{N^r}$ is the flux of dissipated energy, that is, the time change of energy per unit area of the membrane expressed in W·m^{-2}. We can calculate the $\left(\phi^r_F\right)_{N^r}$ and $\left(\phi^r_U\right)_{N^r}$ for the concentration polarization conditions, using the equation:

$$\left[\left(e^r_{ij}\right)_{N^r}\right]_{\max} = \frac{\left[\left(\phi^r_F\right)_{N^r}\right]_{ij}}{\left(\phi^r_U\right)_{N^r}} = \frac{\left[\left(\phi^r_F\right)_{N^r}\right]_{ij}}{\left[\left(\phi^r_F\right)_{N^r}\right]_{ij} + \left(\phi^r_S\right)_{N^r}} \tag{28}$$

By transforming Eq. (28), we get:

$$\left[\left(\phi^r_F\right)_{N^r}\right]_{ij} = \frac{\left[\left(e^r_{ij}\right)_{N^r}\right]_{\max}}{1-\left[\left(e^r_{ij}\right)_{N^r}\right]_{\max}}\left(\phi^r_S\right)_{N^r} \tag{29}$$

where $\left[\left(e^r_{ij}\right)_{N^r}\right]_{\max}$ is the energy conversion efficiency defined by means of Kedem–Caplan–Peusner coefficients [28,52,53] and can be presented in the following form.

$$\left[\left(e^r_{ij}\right)_{N^r}\right]_{\max} = \frac{N^r_{ij}N^r_{ji}}{N^r_{ii}N^r_{jj}\left(1+\sqrt{1-\frac{N^r_{ij}N^r_{ji}}{N^r_{ii}N^r_{jj}}}\right)^2} \tag{30}$$

The values of the coefficients $\left[\left(e^r_{ij}\right)_{N^r}\right]_{\max}$ are limited by the relation $0 \le \left[\left(e^r_{ij}\right)_{N^r}\right]_{\max} \le +1$. Taking into account Eq. (30) in (29) we get:

$$\left[\left(\phi^r_F\right)_{N^r}\right]_{ij} = \frac{N^r_{ij}N^r_{ji}}{N^r_{ii}N^r_{jj}\left(1+\sqrt{1-\frac{N^r_{ij}N^r_{ji}}{N^r_{ii}N^r_{jj}}}\right)^2 - N^r_{ij}N^r_{ji}}\left(\phi^r_S\right)_{N^r} \tag{31}$$

To obtain the equation for $\left(\phi^r_U\right)_{N^r}$ it is necessary to take into consideration Eq. (29) in Eq. (25). After performing the necessary transformations, we get:

$$\left[\left(\phi^r_U\right)_{N^r}\right]_{ij} = \frac{1}{1-\left[\left(e^r_{ij}\right)_{N^r}\right]_{\max}}\left(\phi^r_S\right)_{N^r} \tag{32}$$

Using Eq. (30), Eq. (32) can be transformed to the form:

$$\left[\left(\phi^r_U\right)_{N^r}\right]_{ij} = N^r_{ii}N^r_{jj}\left(1+\sqrt{1-\frac{N^r_{ij}N^r_{ji}}{N^r_{ii}N^r_{jj}}}\right)^2 \left[N^r_{ii}N^r_{jj}\left(1+\sqrt{1-\frac{N^r_{ij}N^r_{ji}}{N^r_{ii}N^r_{jj}}}\right)^2 - N^r_{ij}N^r_{ji}\right]^{-1}\left(\phi^r_S\right)_{N^r} \tag{33}$$

From the above procedure, based on Eqs. (31)–(33), we can calculate the amount of available *F*-energy that can be

converted into useful work and the total internal *U*-energy. It should be noted that in order to obtain Eqs. (11)–(22) for the conditions of homogeneity of solutions, it is sufficient to omit the superscript "*r*" in these equations.

3. Results and discussion

3.1. Calculations of the coefficients N_{ij}, N_{ij}^r and $N_{\det}^r$

The values of the coefficients N_{ij}, N_{ij}^r, $N_{\det}^r$ ($i, j \in \{1, 2, 3\}$, r = A, B) were calculated based on Eqs. (7)–(9) and (12) for glucose in aqueous ethanol solutions and Nephrophan membrane. Eqs. (7)–(9) and (12) show the practical coefficients describing the transport properties of the membrane (L_p, σ_1, σ_2, ω_{11}, ω_{22}, ω_{21} and ω_{12}), the average concentrations of substances "1" and "2" in the membrane ($\bar{C}_1$, $\bar{C}_2$) and the concentration polarization coefficients (ζ_p^r, ζ_{a1}^r, ζ_{a2}^r, ζ_{v1}^r, ζ_{s11}^r, ζ_{s12}^r, ζ_{v2}^r, ζ_{s22}^r and ζ_{s21}^r). The values of these coefficients were determined using the following conditions: $\zeta_p^r = 1$, $\zeta_{ak}^r = 1$, ζ_{v}^r, $\zeta_{s11}^r = \zeta_{s12}^r = \zeta_1^r$ and $\zeta_{s22}^r = \zeta_{s21}^r = \zeta_2^r$ [23,24]. Dependencies $\zeta_v^r = f(\Delta\pi_1)$, $\zeta_k^r = f(\Delta\pi_1)$ and $\zeta_{ak}^r = f(\Delta\pi_1)$ (k = 1, 2 and r = A, B) are presented in Table 1. The dependencies $N_{ij}^r = f(\Delta\pi_1)$ for $\Delta\pi_2$ = 490.2 kPa and {*i*, *j*} Ì ({1, 1}, {2, 1}, {1, 3}, {2, 2}) are presented in Fig. 2.

Fig. 2a shows the dependence $N_{11}^r = f(\Delta\pi_1)$ for $\Delta\pi_2$ = 490.2 kPa. From this figure it results that for homogeneous solution, the value of N_{11}^r is linearly dependent on $\Delta\pi_1$ and independent of the membrane system configuration. This case is illustrated by curves 1A and 1B. For concentration polarization conditions, the value of the N_{11}^r coefficient is nonlinearly dependent on both $\Delta\pi_1$ and the configuration of the membrane system, as is illustrated by curves 2A and 2B. Curve 2A shows that for increase of $\Delta\pi_1$, the value of N_{11}^A decreases nonlinearly from 0.82 × 10^{12} N·s·m^{-3} (for $\Delta\pi_1$ = –171.57 kPa) to 0.22 × 10^{12} N·s·m^{-3} (for $\Delta\pi_1$ = –72.2 kPa) and then from $\Delta\pi_1$ > –72.2 kPa it decreases more slowly to a value of N_{11}^A = 0.2 × 10^{12} N·s·m^{-3}. This can be caused by the fact that for $\Delta\pi_1$ lower than –73.5 kPa ($|\Delta\pi_1|$ > 73.5 kPa) we observe instability region in CBLs, while for $\Delta\pi_1$ higher than –73.5 kPa ($|\Delta\pi_1|$ < 73.5 kPa) stability region of CBLs. Curve 2B, on the other hand, shows that as the value of $\Delta\pi_1$ increases, the value of N_{11}^r initially increases and reaches the maximum value of N_{11}^B = 0.51 × 10^{12} N·s·m^{-3} (for $\Delta\pi_1$ = 37.5 kPa), and then decreases to the value of N_{11}^B = 0.22 × 10^{12} N·s·m^{-3} (for $\Delta\pi_1$ = 101.2 kPa) and then increases linearly to the value N_{11}^r = 0.24 × 10^{12} N·s·m^{-3}, (for $\Delta\pi_1$ > 171.57 kPa). For $\Delta\pi_1$ lower than 73.5 kPa and greater than zero we observe the region of hydrodynamic stability of CBLs while for $\Delta\pi_1$ greater than 73.5 kPa the CBLs can be hydrodynamically instable. It means that in addition to diffusion, convective Rayleigh–Benard movements may occur in CBLs, which may significantly affect the conditions of transport through the membrane. Disregarding the minus sign for $\Delta\pi_1$ (i.e., for $|\Delta\pi_1|$), curves 2A and 2B intersect at the coordinates $|\Delta\pi_1|$ = 78.75 kPa and $N_{11}^A = N_{11}^B$ = 0.26 × 10^{12} N·s·m^{-3}. This is approximately in the transition region between the

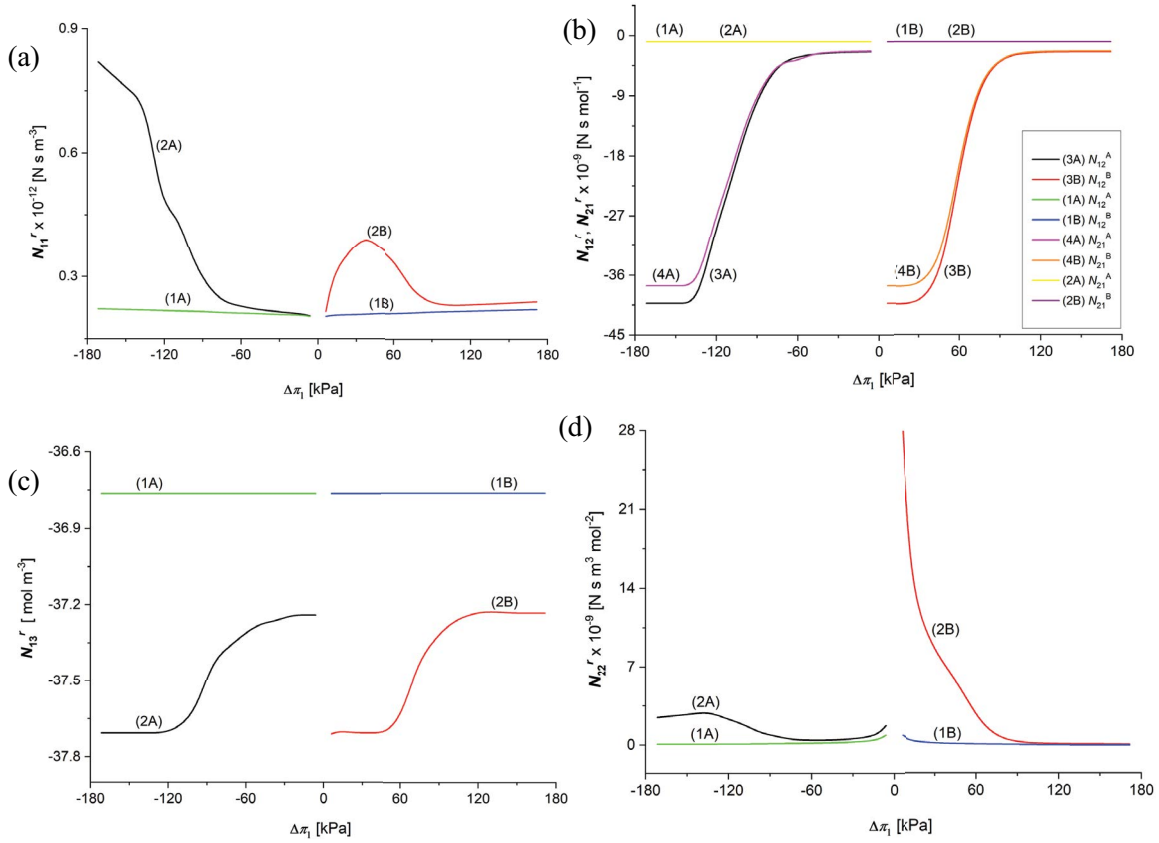

Fig. 2. Coefficients N_{ij}^r ($i, j \in \{1, 2, 3\}$, r = A, B) as functions of glucose osmotic pressure difference ($\Delta\pi_1$) for constant ethanol osmotic pressure difference ($\Delta\pi_2$ = 490.2 kPa): N_{11}^r (a), N_{12}^r and N_{21}^r (b), N_{13}^r (c), and N_{22}^r (d).

stable and unstable range for a given configuration and it means that for this point the value of N^r_{11} is independent of the configuration of the membrane system.

Fig. 2b shows the dependencies $N^r_{12} = f(\Delta\pi_1)$ and $N^r_{21} = f(\Delta\pi_1)$ for $\Delta\pi_2$ = 490.2 kPa. Curves 1A, 1B, 2A and 2B were obtained for homogeneous solution conditions and are symmetric about the vertical axis passing through the point $\Delta\pi_1 = 0$. On the other hand, curves 3A, 3B, 4A and 4B, which illustrate the relationships $N^r_{12} = f(\Delta\pi_1)$ and $N^r_{21} = f(\Delta\pi_1)$ for $\Delta\pi_2$ = 490.2 kPa and for polarization concentration conditions, are characterized by asymmetry about the vertical axis passing through the point $\Delta\pi_1 = 0$. The values of the coefficients N^r_{12} and N^r_{21} are negative for both solutions: homogeneous and under concentration polarization conditions. Similarly, to the N^A_{11} and N^B_{11} coefficients (for $|\Delta\pi_1|$), curves 3A, 3B, 4A and 4B intersect at the point with coordinates $|\Delta\pi_1|$ = 78.75 kPa and $N^A_{12} = N^B_{12} = N^A_{21} = N^B_{21} = -7.28 \times 10^9$ N·s·mol^{-1}. This means that for this point, the values of N^r_{12} and N^r_{21} do not depend on the configuration of the membrane system.

Fig. 2c shows the dependencies $N^r_{13} = f(\Delta\pi_1)$ for $\Delta\pi_2$ = 490.2 kPa. For the homogeneity conditions, the coefficient N^r_{13} does not depend on the glucose concentration and configuration of the membrane system and is equal to $N^r_{13} = -36.76$ mol·m^{-3}. This case is illustrated in this figure by curves 1A and 1B. For the conditions of concentration polarization, the values of the coefficient N^r_{13} are nonlinearly dependent on both $\Delta\pi_1$ and the configuration of the membrane system, as is illustrated by curves 2A and 2B. These graphs show that as the value of $\Delta\pi_1$ increases, the values of N^r_{13} are initially constant and amount to $N^r_{13} = -37.6$ mol·m^{-3}, and then for $\Delta\pi_1 \geq -99.37$ kPa and $\Delta\pi_1 \geq 50.62$ kPa increases to $N^r_{13} = -37.3$ mol·m^{-3}. It should be noted that the coefficient N^r_{13} is negative. The curves 1A and 1B intersect at the point with coordinates $|\Delta\pi_1|$ = 78.75 kPa and $N^A_{13} = N^B_{13} = -37.4$ mol·m^{-3}. This is the osmotic pressure of glucose in the range between the stable and unstable conditions of CBLs. For this point the values of N^A_{13} and N^B_{13} are the same for configurations A and B of the membrane system.

Fig. 2d shows the dependence $N^r_{22} = f(\Delta\pi_1)$ for $\Delta\pi_2$ = 490.2 kPa. Curves 1A and 1B illustrate this dependence for homogeneous solution and for configurations A and B of the membrane system. Curves 1A and 1B are symmetrical, and curves 2A and 2B are asymmetrical with respect to the vertical axis passing through the point $\Delta\pi_1 = 0$. Curve 2A shows that N^A_{22} reaches a maximum value at the $\Delta\pi_1 = -135.9$ kPa point. For $\Delta\pi_1 > -135.9$ kPa, N^r_{22} decreases nonlinearly up to 0.4×10^9 N·s·m^3·mol^{-2}. Curve 2B, on the other hand, shows that N^r_{22} decreases nonlinearly from 27.94×10^9 N·s·m^3·mol^{-2} to 0.83×10^9 N·s·m^3·mol^{-2}. For $\Delta\pi_1 > 78.75$ kPa the coefficient N^r_{22} is constant.

Fig. 3a shows the dependencies $N^r_{23} = f(\Delta\pi_1)$ for $\Delta\pi_2$ = 490.2 kPa. The figure shows that for homogeneous solutions and concentration polarization of the membrane, the N^r_{23} coefficients are concentration-dependent but do not dependent on the configuration of the membrane

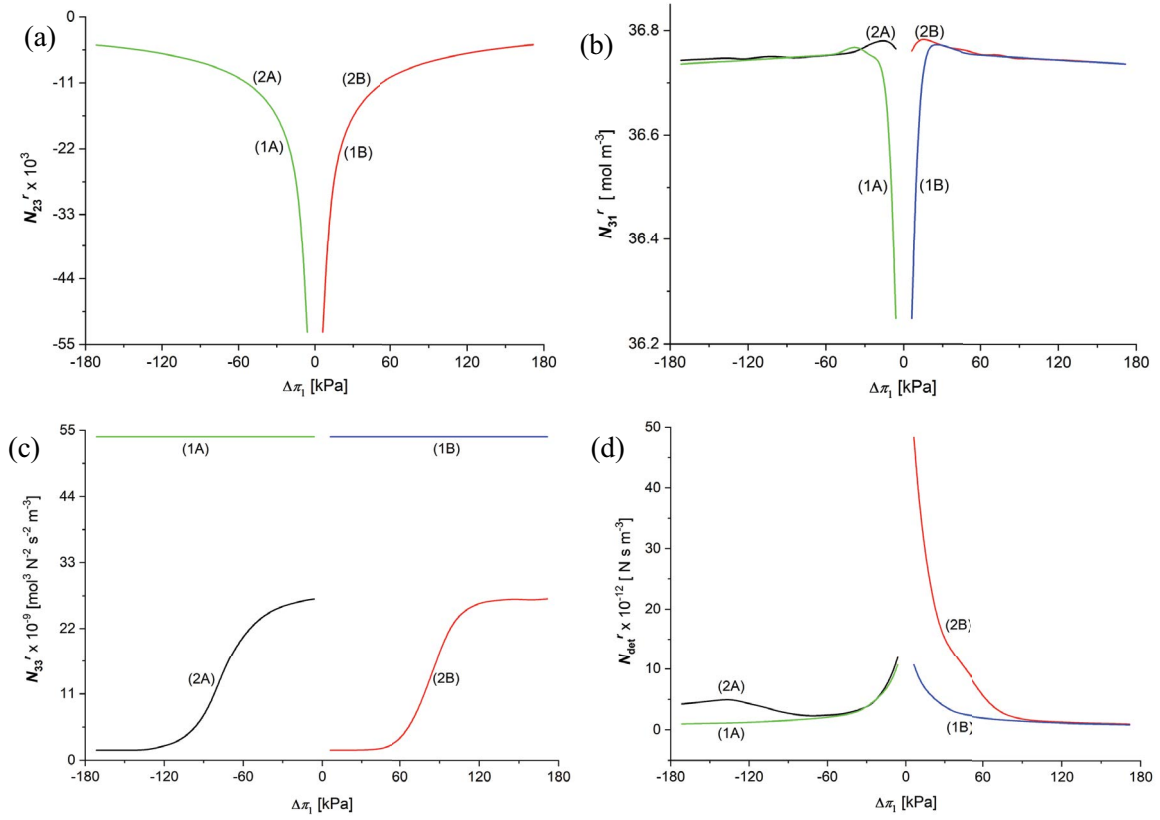

Fig. 3. Coefficients N^r_{ij} and N^r_{det} ($i, j \in \{1, 2, 3\}$, r = A, B) as functions of glucose osmotic pressure difference ($\Delta\pi_1$) for constant ethanol osmotic pressure difference ($\Delta\pi_2$ = 490.2 kPa): N^r_{23} (a), N^r_{31} (b), N^r_{33} (c), and N^r_{det} (d).

system. This case is illustrated by the overlapping nonlinear curves 1A and 2A and 1B and 2B suitably. These curves are symmetric with respect to the vertical axis passing through the point $\Delta\pi_1 = 0$. Unlike the N^r_{23} coefficient, the value of the N^r_{32} coefficient is constant and equal 2.04×10^{-3}.

Fig. 3b shows the relationship $N^r_{31} = f(\Delta\pi_1)$ for $\Delta\pi_2 = 490.2$ kPa. For homogeneous solutions, the value of N^r_{31} decreases nonlinearly with increase of $\Delta\pi_1$ and does not depend on the configuration of the membrane system. This case is illustrated in Fig. 3b by curves 1A and 1B. For concentration polarization conditions, the N^r_{31} coefficients are slightly dependent on $\Delta\pi_1$ and do not depend on the configuration of the membrane system, as is illustrated by curves 2A and 2B. The N^r_{31} coefficient is positive over the entire range of studied $\Delta\pi_1$. Both curves 1A and 1B and curves 2A and 2B are symmetrical with respect to the vertical axis passing through $\Delta\pi_1 = 0$.

Fig. 3c shows the relationship $N^r_{33} = f(\Delta\pi_1)$ for $\Delta\pi_2 = 490.2$ kPa. For homogeneous solutions, N^r_{33} coefficients do not depend on the glucose concentration and configuration of the membrane system and are constant, $N^r_{33} = 53.9 \times 10^9$ m^3·N·s·mol^{-2} (Fig. 3c, curves 1A and 1B). For concentration polarization conditions, the N^r_{33} coefficients depend nonlinearly on both $\Delta\pi_1$ and the configuration of the membrane system, as is illustrated by curves 2A and 2B. Curve 2A shows that as $\Delta\pi_1$ increases, the value of N^r_{33} is initially constant, $N^r_{33} = 1.67 \times 10^9$ m^3·N·s·mol^{-2}, and then for $\Delta\pi_1 > -106.7$ kPa, N^r_{33} increases to 26.9×10^9 m^3·N·s·mol^{-2} (for $\Delta\pi_1 \geq -6.13$ kPa). Similarly, it can be seen from curve 2B that as $\Delta\pi_1$ increases, the value of N^r_{33} is initially constant, $N^r_{33} = 1.67 \times 10^9$ m^3·N·s·mol^{-2}, and then for $\Delta\pi_1 > 59.05$ kPa N^r_{33} increases to the value 26.96×10^9 m^3·N·s·mol^{-2} (for $\Delta\pi_1 \geq 134.05$ kPa). The N^r_{33} coefficients are positive. In addition, curves 2A and 2B intersect at a point with coordinates $|\Delta\pi_1| = 78.75$ kPa and $N^r_{33} = 12.14 \times 10^9$ m^3·N·s·mol^{-2}. For this value of the osmotic pressure difference of glucose, the densities of solutions on both sides of the membrane are similar ($\rho_l \approx \rho_h$). For this point, the values of N^r_{33} are the same for configurations A and B of the membrane system.

Fig. 3d shows the relationship $N^r_{\text{det}} = f(\Delta\pi_1)$ for $\Delta\pi_2 = 490.2$ kPa. Curves 1A an 1B illustrating this relationship for homogeneous solutions are nonlinear curves and N^r_{det} does not depend on the configuration of the membrane system. Curves 2A and 2B for concentration polarization conditions are asymmetric with respect to the axis passing through the point $\Delta\pi_1 = 0$. These curves also show that the value of N^r_{det} depends nonlinearly on both $\Delta\pi_1 = 0$, as well as on the configuration of the membrane system. Curves 2A and 2B intersect at the point with coordinates $|\Delta\pi_1| = 73.04$ kPa and $N^A_{\text{det}} = N^B_{\text{det}} = 2.85 \times 10^{12}$ N·s·m^{-3}. This means that for this point the values of N^A_{det} and N^B_{det} are the same for configurations A and B of the membrane system.

3.2. Calculations of the energy dissipation (S-energy) $\left(\varphi^r_S\right)_{N^r}$

Eq. (27) shows that the knowledge of the N^r_{ij} coefficients and J^r_{s1}, J^r_v and J^r_{s2} fluxes is required to calculate $\left(\varphi^r_S\right)_{N^r}$. Fig. 4a shows the dependencies $\left(\varphi^r_S\right)_{N^r} = f(\Delta\pi_1)$ for $\Delta\pi_2 = 490.2$ kPa, calculated on the basis of this equation. The dependencies $N^r_{ij} = f(\Delta\pi_1)$ for $\Delta\pi_2 = 490.2$ kPa, ($i, j \in \{1, 2, 3\}$, r = A, B) are shown in Figs. 2a–d and 3a–c. The experimentally determined values of J^r_{s1}, J^r_v and J^r_{s2} are summarized in Tables 2 and 3.

Curves 1A and 1B illustrate the dependence $\left(\varphi^r_S\right)_{N^r} = f(\Delta\pi_1)$ for $\Delta\pi_2 = 490.2$ kPa and for the homogeneity conditions of the solutions and configurations A and B of the membrane system.

Curves 1A and 1B indicate that $\left(\varphi^r_S\right)_{N^r}$ is concentration-dependent and configuration-independent, and the value of $\left(\varphi^r_S\right)_{N^r}$, in the range of studied $\Delta\pi_1$, increases from 0.02 to 1.41 W·m^{-2}. For the concentration polarization conditions, the $\left(\varphi^r_S\right)_{N^r} = f(\Delta\pi_1)$ is nonlinear and depends on both $\Delta\pi_1$ and configuration of the membrane system, what is illustrated by the curves 2A and 2B. Curves 2A and 2B are asymmetrical with respect to the vertical axis passing through the point $\Delta\pi_1 = 0$. Moreover, for the same values of $\Delta\pi_1$, the $\left(\varphi^A_S\right)_{N^r}$ and $\left(\varphi^B_S\right)_{N^r}$ values illustrated by curves 2A and 2B are much smaller in comparison to curves 1A and 1B.

3.3. Osmotic pressure dependencies of $\left[\left(e^r_{ij}\right)_{N^r}\right]_{\max}$

Fig. 4b–d show the dependencies $\left[\left(e^r_{ij}\right)_{N^r}\right]_{\max} = f(\Delta\pi_1)$ for $\Delta\pi_2 = 490.2$ kPa ($i, j \in \{1, 2, 3\}$, r = A, B) calculated on the basis of Eq. (19) and data presented in Figs. 2a–d and 3a–c. It can be seen from Fig. 4b that the values of the coefficients $\left[\left(e^A_{12}\right)_{N^r}\right]_{\max}$ and $\left[\left(e^A_{21}\right)_{N^r}\right]_{\max}$ illustrated by curves 3A and 4A for concentration polarization conditions and configuration A, decrease nonlinearly with $\Delta\pi_1$ increase. On the other hand, the values of coefficients $\left[\left(e^A_{12}\right)_{N^r}\right]_{\max}$ and $\left[\left(e^A_{21}\right)_{N^r}\right]_{\max}$ for homogeneous solutions decrease linearly with the increase of $\Delta\pi_1$.

For the conditions of concentration polarization and configuration B of the membrane system, the values of the coefficients $\left[\left(e^B_{12}\right)_{N^r}\right]_{\max}$ and $\left[\left(e^B_{21}\right)_{N^r}\right]_{\max}$ initially increase nonlinearly with increase of $\Delta\pi_1$ and reach maximal values: $\left[\left(e^B_{12}\right)_{N^r}\right]_{\max} = 0.39$ (curve 3B) and $\left[\left(e^B_{21}\right)_{N^r}\right]_{\max} = 0.34$ (curve 4B) for $\Delta\pi_1 = 50.6$ kPa. Next, they decrease to a constant and minimal values. Graphs 1A, 1B, 2A and 2B obtained for homogeneity of solutions are symmetrical with respect to the vertical axis passing through the point $\Delta\pi_1 = 0$ and $\left[\left(e^A_{12}\right)_{N^r}\right]_{\max} = \left[\left(e^B_{21}\right)_{N^r}\right]_{\max} = \left[\left(e^B_{12}\right)_{N^r}\right]_{\max} = \left[\left(e^B_{21}\right)_{N^r}\right]_{\max} = \left[\left(e^B_{12}\right)_{N^r}\right]_{\max} = \left[\left(e_{21}\right)_{N^r}\right]_{\max}$. On the other hand, graphs 3A and 3B and 4A and 4B obtained for the concentration polarization conditions of the solutions are asymmetric about the vertical axis passing through the point $\Delta\pi_1 = 0$, $\left[\left(e^A_{12}\right)_{N^r}\right]_{\max} > \left[\left(e^A_{21}\right)_{N^r}\right]_{\max} > \left[\left(e_{12}\right)_{N^r}\right]_{\max} = \left[\left(e_{21}\right)_{N^r}\right]_{\max}$ and $\left[\left(e^B_{12}\right)_{N^r}\right]_{\max} > \left[\left(e^B_{21}\right)_{N^r}\right]_{\max} > \left[\left(e_{12}\right)_{N^r}\right]_{\max} = \left[\left(e_{21}\right)_{N^r}\right]_{\max}$.

From curves 1A, 1B, 2A and 2B shown in Fig. 4c, it can be seen that for homogeneous solutions, the values of the coefficients $\left[\left(e^A_{13}\right)_{N^r}\right]_{\max}$, $\left[\left(e^A_{31}\right)_{N^r}\right]_{\max}$, $\left[\left(e^B_{13}\right)_{N^r}\right]_{\max}$, $\left[\left(e^B_{31}\right)_{N^r}\right]_{\max}$ do not depend on $\Delta\pi_1$ and configurations A and B of the membrane system. Moreover, the condition

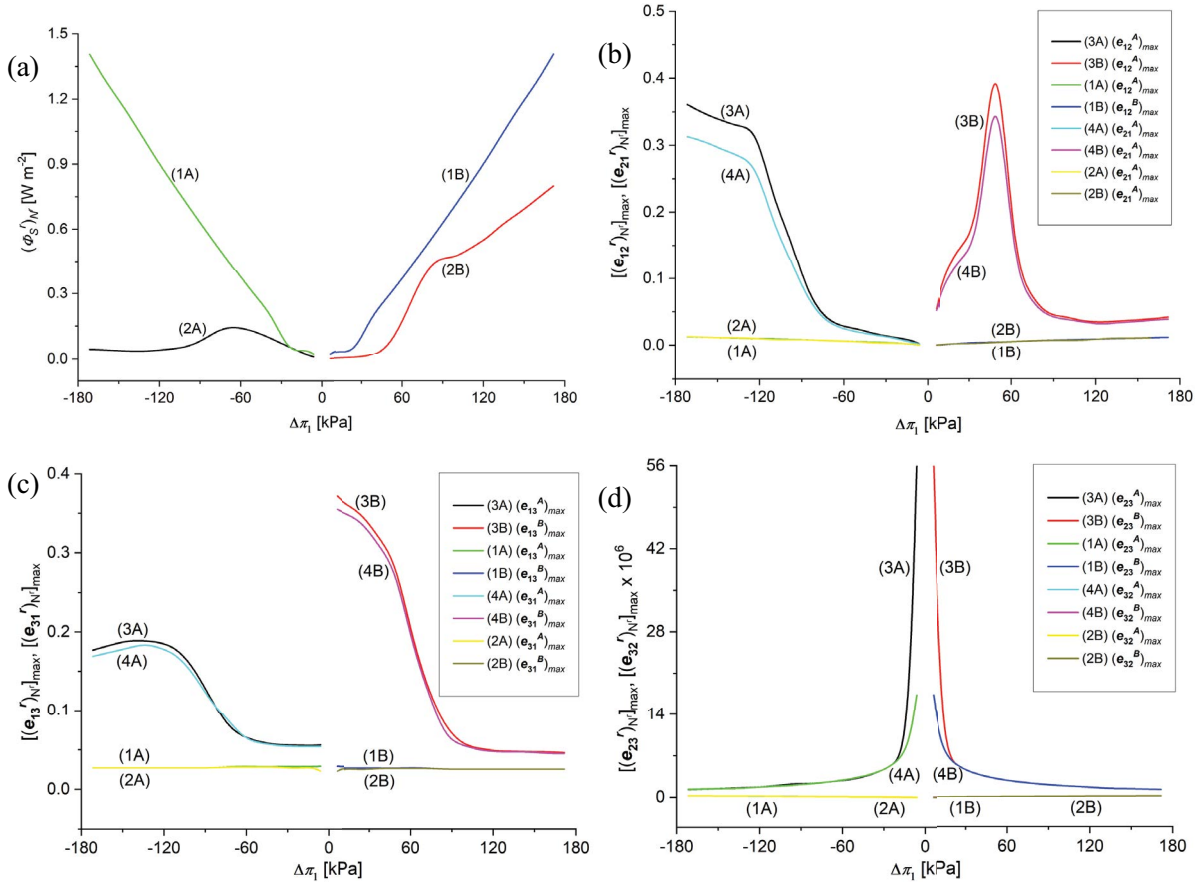

Fig. 4. Energy dissipation $\left(\varphi_S^r\right)_{N^r}$ (r = A, B), S-energy) as function of glucose osmotic pressure difference ($\Delta\pi_1$) for constant ethanol osmotic pressure difference $\Delta\pi_2$ = 490.2 kPa (a), $\left[\left(e_{ij}^r\right)_{N^r}\right]_{\max}$ coefficients (r = A, B) as functions of glucose osmotic pressure difference ($\Delta\pi_1$) for $\Delta\pi_2$ = 490.2 kPa and for (i, j) = {(1, 2) and (2, 1) (b), (1, 3) and (3, 1) (c) and (2, 3) and (3, 2) (d)}.

Table 2
Values of volume (J_v^A, J_v^B), glucose (J_1^A, J_1^B) and ethanol (J_2^A, J_2^B) fluxes of homogeneity solutions for Nephrophan membrane [41]

$\Delta\pi_1$ (kPa)	Homogeneous solutions						
	J_v^A (nm·s^{-1})	J_1^A (μmol·m^{-2}·s^{-1})	J_2^A (μmol·m^{-2}·s^{-1})	$\Delta\pi_1$ (kPa)	J_v^B (nm·s^{-1})	J_1^B (μmol·m^{-2}·s^{-1})	J_2^B (μmol·m^{-2}·s^{-1})
–171.57	–117.2	–137.3	–701.1	0	60.0	–	–
–159.31	–113.1	–127.5	–701.1	6.13	62.1	4.9	701.1
–147.06	–109.0	–117.7	–701.1	12.25	64.1	9.8	701.1
–134.05	–105.0	–107.9	–701.1	24.51	68.2	19.6	701.1
–122.55	–100.9	–98.0	–701.1	36. 76	72.3	29.4	701.1
–110.29	–96.8	–88.2	–701.1	49.02	76.4	39.2	701.1
–98.04	–92.7	–78.4	–701.1	61.27	80.5	49.1	701.1
–85.78	–88.6	–68.6	–701.1	73.53	84.5	58.8	701.1
–73.53	–84.5	–58.8	–701.1	85.78	88.6	68.6	701.1
–61.27	–80.5	–49.1	–701.1	98.04	92.7	78.4	701.1
–49.02	–76.4	–39.2	–701.1	110.29	96.8	88.2	701.1
–36. 76	–72.3	–29.4	–701.1	122.55	100.9	98.0	701.1
–24.51	–68.2	–9.6	–701.1	134.05	100.5	107.9	701.1
–12.25	–64.1	–9.8	–701.1	147.06	109.0	117.7	701.1
–6.13	–62.1	–4.9	–701.1	159.31	113.1	127.5	701.1
0	–60.0	–	–	171.57	117.2	137.3	701.1

Table 3
Values of volume (J_v^A, J_v^B), glucose (J_1^A, J_1^B) and ethanol (J_2^A, J_2^B) fluxes of non-homogeneity solutions for Nephrophan membrane [41]

$\Delta\pi_1$ (kPa)	Non-homogeneous solutions						
	J_v^A (nm·s^{-1})	J_1^A (μmol·m^{-2}·s^{-1})	J_2^A (μmol·m^{-2}·s^{-1})	$\Delta\pi_1$ (kPa)	J_v^B (nm·s^{-1})	J_1^B (μmol·m^{-2}·s^{-1})	J_2^B (μmol·m^{-2}·s^{-1})
–171.57	–3.6	4	–22.7	0	1.91	–	–
–159.31	–3.5	0.25	–21.7	6.13	1.92	0.1	21.7
–147.06	–3.4	–3.95	–21.7	12.25	1.93	0.3	21.7
–134.05	–3.2	–3.65	–22.4	24.51	2.11	0.6	21.7
–122.55	–4.1	–3.34	–25.9	36.76	2.31	0.9	21.7
–110.29	–5.3	–4.02	–47.0	49.02	2.82	1.4	28.7
–98.04	–8.4	–4.85	–105.2	61.27	5.39	3.2	38.5
–85.78	–14.2	–7.14	–203.3	73.53	12.7	8.8	63.8
–73.53	–24.9	–10.98	–294.4	85.78	25.7	19.9	112.2
–61.27	–30.6	–17.36	–329.5	98.04	38.9	32.9	206.8
–49.02	–32.9	–18.64	–343.5	110.29	43.5	41.5	206.4
–36. 76	–33.8	–17.06	–347.0	122.55	49.0	48.1	305.0
–24.51	–33.1	–13.77	–349.8	134.05	51.9	53.4	328.0
–12.25	–31.8	–9.51	–349.8	147.06	54.6	58.8	340.0
–6.13	–31.1	–4.86	–349.8	159.31	56.6	63.7	347.7
0	–30.2	–2.45	–	171.57	58.65	68.6	350.5

$\left(e_{13}^A\right)_{N^r} = \left(e_{31}^A\right)_{N^r} = \left[\left(e_{13}^B\right)_{N^r}\right]_{\max} = \left[\left(e_{31}^B\right)_{N^r}\right]_{\max}$ is satisfied. On the other hand, for concentration polarization conditions and configuration A, the coefficients $\left[\left(e_{13}^A\right)_{N^r}\right]_{\max}$, $\left[\left(e_{31}^A\right)_{N^r}\right]_{\max}$, $\left[\left(e_{13}^B\right)_{N^r}\right]_{\max}$, $\left[\left(e_{31}^B\right)_{N^r}\right]_{\max}$ initially increase to the maximal value $\left[\left(e_{13}^A\right)_{N^r}\right]_{\max}$, $\left[\left(e_{31}^A\right)_{N^r}\right]_{\max} \approx \left[\left(e_{31}^A\right)_{N^r}\right]_{\max} = 0.19$ for $\Delta\pi_1$ = –134.1 kPa. Then, for $\Delta\pi_1$ > –134.1 kPa, the values of $\left[\left(e_{13}^A\right)_{N^r}\right]_{\max}$ and $\left[\left(e_{31}^A\right)_{N^r}\right]_{\max}$ decrease to the minimal value $\left[\left(e_{13}^A\right)_{N^r}\right]_{\max} = \left[\left(e_{31}^A\right)_{N^r}\right]_{\max} = 0.029$. For configuration B, the values of $\left[\left(e_{13}^B\right)_{N^r}\right]_{\max}$ and $\left[\left(e_{31}^B\right)_{N^r}\right]_{\max}$ decrease nonlinearly to a constant and minimum value $\left[\left(e_{13}^B\right)_{N^r}\right]_{\max} = \left[\left(e_{31}^B\right)_{N^r}\right]_{\max} = 0.05$. It can be shown that curves 3A and 3B and 4A and 4B intersect at the point with coordinates $\Delta\pi_1$ = ±80.6 kPa and $\left[\left(e_{13}^A\right)_{N^r}\right]_{\max} = \left[\left(e_{31}^A\right)_{N^r}\right]_{\max} = \left[\left(e_{13}^B\right)_{N^r}\right]_{\max} = \left[\left(e_{31}^B\right)_{N^r}\right]_{\max}$. This point is in a range of $\Delta\pi_1$ between the areas of hydrodynamic stability and instability of the CBLs. In this point, the coefficients $\left[\left(e_{13}^A\right)_{N^r}\right]_{\max} = \left[\left(e_{31}^A\right)_{N^r}\right]_{\max} = \left[\left(e_{13}^B\right)_{N^r}\right]_{\max} = \left[\left(e_{31}^B\right)_{N^r}\right]_{\max}$ for concentration polarization conditions, do not depend on the configuration of the membrane system.

Fig. 4d shows the dependencies $\left[\left(e_{23}^r\right)_{N^r}\right]_{\max} = f(\Delta\pi_1)$ and $\left[\left(e_{32}^r\right)_{N^r}\right]_{\max} = f(\Delta\pi_1)$ for $\Delta\pi_2$ = 490.2 kPa (r = A, B), respectively. Curves 1A and 1B in this figure illustrate this dependence for homogeneous solutions. For concentration polarization conditions, the value of the coefficient $\left(e_{23}^r\right)_{N^r}$ is nonlinearly dependent on $\Delta\pi_1$, and do not depend on the configurations A and B of the membrane system, as is illustrated by curves 1A, 1B, 2A and 2B. In addition, all graphs are pairwise symmetric, with respect to the vertical axis passing through the point $\Delta\pi_1$ = 0, and independent of the configuration of the membrane system.

3.4. Calculations of F-energy and U-energy in the membrane system

Fig. 5 shows the relationship $\left[\left(\phi_F^r\right)_{N^r}\right]_{ij} = f(\Delta\pi_1)$ for $\Delta\pi_2$ = 490.2 kPa, calculated from Eq. (18). Curves 1 and 2 shown in Fig. 5a illustrate the dependencies $\left[\left(\phi_F^r\right)_{N^r}\right]_{12} = f(\Delta\pi_1$ and $\left[\left(\phi_F^r\right)_{N^r}\right]_{21} = f(\Delta\pi_1)$ for $\Delta\pi_2$ = 490.2 kPa, for homogeneous solutions and configurations A (left branches of the curve) and B (right branches of the curve). The aforementioned relations for homogeneous solutions are symmetric nonlinear curves independent on the configuration of the membrane system.

For concentration polarization conditions, the dependencies $\left[\left(\phi_F^r\right)_{N^r}\right]_{12} = f(\Delta\pi_1)$ and $\left[\left(\phi_F^r\right)_{N^r}\right]_{21} = f(\Delta\pi_1)$ for $\Delta\pi_2$ = 490.2 kPa, are the curves 3A and 4A, with the curve 4A located above the curve 3A. In contrast, the relations $\left[\left(\phi_F^B\right)_{N^r}\right]_{12} = f(\Delta\pi_1)$ and $\left[\left(\phi_F^B\right)_{N^r}\right]_{21} = f(\Delta\pi_1)$ for $\Delta\pi_2$ = 490.2 kPa, are complex curves 3B and 4B with distinct two extremes. The maximum of curve 3B has coordinates $\Delta\pi_1$ = 50.6 kPa and $\left[\left(\phi_F^B\right)_{N^r}\right]_{21}$ = 0.034 W·m^{-2} and the maximum of curve 4B has coordinates $\Delta\pi_1$ = 46.9 kPa and $\left[\left(\phi_F^B\right)_{N^r}\right]_{21}$ = 0.046 W·m^{-2}. On the other hand, the minimum of curve 3B has coordinates $\Delta\pi_1$ = 117.2 kPa and $\left[\left(\phi_F^B\right)_{N^r}\right]_{21}$ = 0.019 and minimum of curve 4B has coordinates $\Delta\pi_1$ = 114.4 kPa and $\left[\left(\phi_F^B\right)_{N^r}\right]_{21}$ = 0.021 W·m^{-2}. From above data it follows, that curves 3A and 3B and 4A and 4B are asymmetric and that the values of $\left[\left(\phi_F^r\right)_{N^r}\right]_{12} = f(\Delta\pi_1$ and $\left[\left(\phi_F^r\right)_{N^r}\right]_{21} = f(\Delta\pi_1$ for $\Delta\pi_2$ = 490.2 kPa are dependent

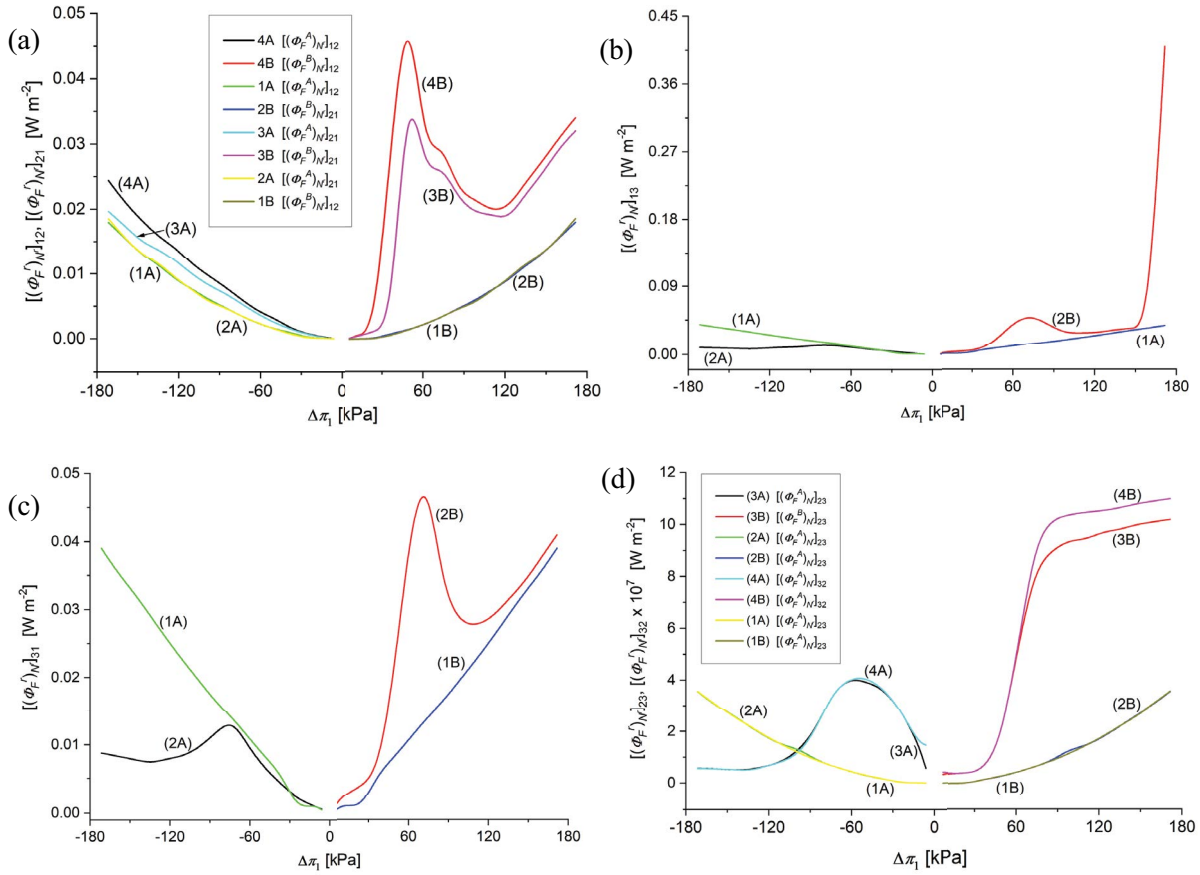

Fig. 5. Total production of free energy $\left[\left(\phi_F^r\right)_{N^r}\right]_{ij}$, for (*i*, *j*) = {(1, 2) and (2, 1) (a), (1, 3) (b) (3, 1) (c), (2, 3) and (3, 2) (d)} and *r* = A, B, as functions of osmotic pressure difference of glucose ($\Delta\pi_1$) with a constant osmotic pressure of ethanol $\Delta\pi_2$ = 490.3 kPa and ΔP = 0.

on the configuration of the membrane system. Curves 1A and 1B shown in Fig. 5b illustrate the linear dependencies $\left[\left(\phi_F^r\right)_{N^r}\right]_{13} = f(\Delta\pi_1)$ for $\Delta\pi_2$ = 490.2 kPa for homogeneous solutions and configurations A and B. The aforementioned relations for homogeneous solution are symmetric straight lines independent of the configuration of the membrane system. For concentration polarization conditions, the relations $\left[\left(\phi_F^r\right)_{N^r}\right]_{13} = f(\Delta\pi_1$ for $\Delta\pi_2$ = 490.2 kPa take the form of curves 2A and 2B and are complex curves with distinct two extremes. It follows that curves 2A and 2B are asymmetric and dependent on the configuration of the membrane system.

The maximum of curve 3B has coordinates $\Delta\pi_1$ = 50.6 kPa and $\left[\left(\phi_F^B\right)_{N^r}\right]_{21}$ = 0.034 W·m^{-2} and maximum of curve 4B has coordinates $\Delta\pi_1$ = 46.9 kPa and $\left[\left(\phi_F^B\right)_{N^r}\right]_{21}$ = 0.046 W·m^{-2}. On the other hand, the minimum of curve 3B has coordinates $\Delta\pi_1$ = 117.2 kPa and $\left[\left(\phi_F^B\right)_{N^r}\right]_{21}$ = 0.019 and minimum of curve 4B has coordinates $\Delta\pi_1$ = 114.4 kPa and $\left[\left(\phi_F^B\right)_{N^r}\right]_{21}$ = 0.021 W·m^{-2}. The curves 3A and 3B and 4A and 4B are asymmetric and the values of $\left[\left(\phi_F^r\right)_{N^r}\right]_{21} = f(\Delta\pi_1$ and $\left[\left(\phi_F^r\right)_{N^r}\right]_{21} = f(\Delta\pi_1)$ for $\Delta\pi_2$ = 490.2 kPa are dependent on the configuration of the membrane system. Curves 1A and 1B shown in Fig. 5b illustrate the linear dependencies $\left[\left(\phi_F^r\right)_{N^r}\right]_{13} = f(\Delta\pi_1)$ for $\Delta\pi_2$ = 490.2 kPa for homogeneous solutions and configurations A and B of the membrane system. The aforementioned relations for homogeneous solutions are symmetric straight lines independent on the configuration of the membrane system. For concentration polarization conditions, the relations $\left[\left(\phi_F^r\right)_{N^r}\right]_{13} = f(\Delta\pi_1)$ for $\Delta\pi_2$ = 490.2 kPa take the form of curves 2A and 2B and are complex curves with distinct two extremes. The curves 2A and 2B are asymmetric and depend on the configuration of the membrane system.

Curves 1A and 1B shown in Fig. 5c illustrate the dependence $\left[\left(\phi_F^r\right)_{N^r}\right]_{13} = f(\Delta\pi_1)$ for $\Delta\pi_2$ = 490.2 kPa for solution homogeneity conditions and configurations A (left branch of the curve) and B (right branch of the curve). The aforementioned relations for homogeneous solutions are symmetric nonlinear curves and do not depend on the configuration of the membrane system. For concentration polarization conditions, the relations $\left[\left(\phi_F^r\right)_{N^r}\right]_{13} = f(\Delta\pi_1)$ for $\Delta\pi_2$ = 490.2 kPa take the form of curves 2A and 2B and are complex curves with distinct two extremes. The maximum of curve 2A has coordinates $\Delta\pi_1$ = 76.9 kPa and $\left[\left(\phi_F^r\right)_{N^r}\right]_{13}$ = 0.013 W·m^{-2}, and maximum of the curve 2B has coordinates $\Delta\pi_1$ = 69.4 kPa and $\left[\left(\phi_F^r\right)_{N^r}\right]_{13}$ = 0.046 W·m^{-2}, while the minimum of curve 2A has coordinates $\Delta\pi_1$ = –133.1 kPa and $\left[\left(\phi_F^A\right)_{N^r}\right]_{31}$ = 0.007,

and minimum of the curve 2B has coordinates = 106.9 kPa and $\left[\left(\phi_F^B\right)_{N^r}\right]_{31}$ = 0.028 W·m^{-2}. It follows that the curves 2A and 2B are asymmetric and depend on the membrane system configuration.

Curves 1 and 2 shown in Fig. 5d illustrate the dependencies $\left[\left(\phi_F^r\right)_{N^r}\right]_{23} = f(\Delta\pi_1)$ and $\left[\left(\phi_F^r\right)_{N^r}\right]_{32} = f(\Delta\pi_1)$ for $\Delta\pi_2$ = 490.2 kPa for of homogeneous solutions and configurations A (left branches of the curves) and B (right branches of the curves). The aforementioned relations for homogeneous solutions are symmetric nonlinear curves independent of the configuration of the membrane system. Moreover, for the same values of $\Delta\pi_1$, $\left[\left(\phi_F^r\right)_{N^r}\right]_{23} = \left[\left(\phi_F^r\right)_{N^r}\right]_{32}$. For concentration polarization conditions, the dependencies $\left[\left(\phi_F^r\right)_{N^r}\right]_{23} = f(\Delta\pi_1)$ and $\left[\left(\phi_F^r\right)_{N^r}\right]_{32} = f(\Delta\pi_1)$ for $\Delta\pi_2$ = 490.2 kPa are shown by the curves 3B and 4B, which are complex curves and curves 3A and 4A which have maxima at points with coordinates $\Delta\pi_1$ = 56.2 kPa and $\left[\left(\phi_F^A\right)_{N^r}\right]_{23}$ = 4.1 × 10^{-7} W·m^{-2} (curve 3A), and $\Delta\pi_1$ = 52.5 kPa and $\left[\left(\phi_F^A\right)_{N^r}\right]_{32}$ = 4.1 × 10^{-7} W·m^{-2} (curve 4A). From the above, it is clear that curves 3A and 3B and 4A and 4B are asymmetric and that the values $\left[\left(\phi_F^r\right)_{N^r}\right]_{23} = f(\Delta\pi_1)$ and $\left[\left(\phi_F^r\right)_{N^r}\right]_{32} = f(\Delta\pi_1)$ for $\Delta\pi_2$ = 490.2 kPa depend on configuration of the membrane system.

Using the dependencies $N_{ij}^r = f(\Delta\pi_1)$ and $N_{\text{det}}^r = f(\Delta\pi_1)$ for $\Delta\pi_2$ = 490.2 kPa ($i, j \in \{1, 2, 3\}$, r = A, B) shown in Figs. 2 and 3, the dependencies $n_{ij}^r = f(\Delta\pi_1)$ for $\Delta\pi_2$ = 490.2 kPa ($i, j \in \{1, 2, 3\}$, $i \neq j$, r = A, B), $\left(Q_{ij}^r\right)_{N^r} = f(\Delta\pi_1)$ for $\Delta\pi_2$ = 490.2 kPa ($i, j \in \{1, 2, 3\}$, $i \neq j$, r = A, B) and $\left(\chi_{ij}\right)_{N^r} = f(\Delta\pi_1)$ for $\Delta\pi_2$ = 490.2 kPa ($i, j \in \{1, 2, 3\}$, $i \neq j$ or $i, j \equiv$ det) were calculated. Besides, the relationships between the Peusner coefficients (N_{ij}^r, N_{det}^r $i \neq j \in \{1, 2, 3\}$, r = A, B) and modified Péclet coefficients ($\wp_{vk}^r$, $\wp_{ak}^r$, k = 1 or 2) will be shown in the next part of the article. The classic Péclet coefficient is expressed by the ratio: the rate of advection and the rate of diffusion [50,51].

3.5. Osmotic pressure dependencies of $\left(n_{ij}^r\right)_{N^r}$

The coefficients n_{12}^r and n_{21}^r are measures of the degree of coupling between the processes ($J_v^r(\Delta P - \Delta\pi_1 - \Delta\pi_2)$) and $\left(J_{S1}^r, \frac{\Delta\pi_1}{\bar{C}_1}\right)$. In turn, the coefficients n_{13}^r and n_{31}^r are measures of the degree of coupling between the processes ($J_v^r(\Delta P - \Delta\pi_1 - \Delta\pi_2)$) and $\left(J_{S2}^r, \frac{\Delta\pi_2}{\bar{C}_2}\right)$ and the coefficients n_{23}^r and n_{32}^r are measures of the degree of coupling of the processes $\left(J_{S1}^r, \frac{\Delta\pi_1}{\bar{C}_1}\right)$ and $\left(J_{S2}^r, \frac{\Delta\pi_2}{\bar{C}_2}\right)$. The values of the n_{ij}^r coefficient:

$$n_{ij}^r = \frac{N_{ij}^r}{\sqrt{N_{ii}^r N_{jj}^r}}, \left(i, j \in \{1,2,3\}, r = A, B\right) \tag{34}$$

can be calculated using above formula and dependencies $N_{ij}^r = f(\Delta\pi_1)$ for $\Delta\pi_2$ = 490.2 kPa presented in Figs. 2a–d and 3a–c.

Klinkman et al. study shows [49] that for homogeneous solutions these coefficients should satisfy the relation $-1 \le n_{ij}^r = n_{ij} \le +1$. If $n_{ij} = 0$, then the processes ($J_v^r(\Delta P - \Delta\pi_1 - \Delta\pi_2)$), $\left(J_{S1}^r, \frac{\Delta\pi_1}{\bar{C}_1}\right)$, ($J_v^r(\Delta P - \Delta\pi_1 - \Delta\pi_2)$), $\left(J_{S2}^r, \frac{\Delta\pi_2}{\bar{C}_2}\right)$, $\left(J_{S1}^r, \frac{\Delta\pi_1}{\bar{C}_1}\right)$ and $\left(J_{S2}^r, \frac{\Delta\pi_2}{\bar{C}_2}\right)$ are not coupled. If $n_{ij} > 0$ the coupling of the processes under consideration leads to a decrease of the fluxes with decrease of coupled stimuli. If $n_{ij} < 0$, then with an increase in the value of the stimulus of one process there is observed a decrease in the flux of the process coupled to it. The value $n_{ij} = \pm 1$ is reached only for full coupling of processes. Fig. 6a shows the dependence $\left[\left(\phi_U^r\right)_{N^r}\right]_{13} = \Delta\pi_1$) for $\Delta\pi_2$ = 490.2 kPa calculated from the Eq. (34). Curves 1 illustrate this relationship for homogeneous solutions and configurations A and B.

From curves 1A and 1B, it can be seen that $\left[\left(\phi_U^r\right)_{N^r}\right]_{13}$ depend on solutions concentration and do not depend on the configuration of the membrane system, and the values of $\left[\left(\phi_U^r\right)_{N^r}\right]_{13}$, in the range of studied $\Delta\pi_1$, increase from 0.02 to 1.44 W·m^{-2}. For concentration polarization conditions, the values of $\left[\left(\phi_U^r\right)_{N^r}\right]_{13}$ is nonlinear and depends on $\Delta\pi_1$ and the configuration of the membrane system, as is illustrated by curves 2A and 2B. Curves 2A and 2B are asymmetrical with respect to the vertical axis passing through the point $\Delta\pi_1$ = 0. Moreover, for the same values of $\Delta\pi_1$, the values of $\left[\left(\phi_U^A\right)_{N^r}\right]_{13}$ and $\left[\left(\phi_U^B\right)_{N^r}\right]_{13}$ illustrated by curves 1A and 1B are much smaller in comparison to curve 1. Very similar results were obtained from calculation for the relationships $\left[\left(\phi_U^r\right)_{N^r}\right]_{13} = f(\Delta\pi_1)$, $\left[\left(\phi_U^r\right)_{N^r}\right]_{31} = f(\Delta\pi_1)$, $\left[\left(\phi_U^r\right)_{N^r}\right]_{23} = f(\Delta\pi_1)$, $\left[\left(\phi_U^r\right)_{N^r}\right]_{32} = f(\Delta\pi_1)$, $\left[\left(\phi_U^r\right)_{N^r}\right]_{12} = f(\Delta\pi_1)$ and $\left[\left(\phi_U^r\right)_{N^r}\right]_{21} = f(\Delta\pi_1)$, in all cases $\Delta\pi_2$ = 490.2 kPa.

Fig. 6b shows that the values of the coefficients $\left(n_{12}^A\right)_{N^r}$ and $\left(n_{21}^A\right)_{N^r}$ for homogeneous solutions and configurations A and B, illustrated by curves 1A, 1B, 2A and 2B, decrease nonlinearly with increasing values of $|\Delta\pi_1|$, and are negative. The curves 1A and 1B and 2A and 2B for homogeneous solutions are symmetrical with respect to the vertical axis passing through the point $\Delta\pi_1$ = 0 and $\left(n_{12}^A\right)_{N^r} = \left(n_{21}^A\right)_{N^r}$ and $\left(n_{12}^B\right)_{N^r} = \left(n_{21}^B\right)_{N^r}$. On the other hand, graphs 3A and 3B and 4A and 4B obtained for concentration polarization conditions are complex curves. They are asymmetric with respect to the vertical axis passing through the point $|\Delta\pi_1|$ = 0. The curves 3A and 4A satisfy the relations $\left(n_{12}^A\right)_{N^r} \approx \left(n_{21}^A\right)_{N^r}$ and the curves 3B and 4B satisfy the relations $\left(n_{12}^B\right)_{N^r} \approx \left(n_{21}^B\right)_{N^r}$. For the conditions of concentration polarization and configuration B, the values of the coefficients $\left(n_{21}^B\right)_{N^r}$ initially decrease nonlinearly and reach minimal values $\left(n_{12}^B\right)_{N^r}$ = –0.88 (curve 3B) and $\left(n_{21}^B\right)_{N^r}$ = 0.81 (curve 4B) for $\Delta\pi_1$ = 45.5 kPa, after which they increase.

Fig. 6c shows the dependencies $\left(n_{13}^r\right)_{N^r}$ and $\left(n_{31}^r\right)_{N^r}$ on $\Delta\pi_1$ for $\Delta\pi_2$ = 490.2 kPa. For homogeneous solutions, the values of these coefficients are independent on the concentration and configuration of the membrane system. The values of these coefficients are $\left(n_{13}^A\right)_{N^r} = \left(n_{13}^B\right)_{N^r}$ = –0.34 (Fig. 6c, curves 1A and 1B) and $\left(n_{31}^A\right)_{N^r} = \left(n_{31}^B\right)_{N^r}$ = 0.34 (Fig. 6c, curves 2A and 2B). For concentration polarization conditions, the values of the coefficients $\left(n_{13}^r\right)_{N^r}$ and $\left(n_{31}^r\right)_{N^r}$ depend nonlinearly

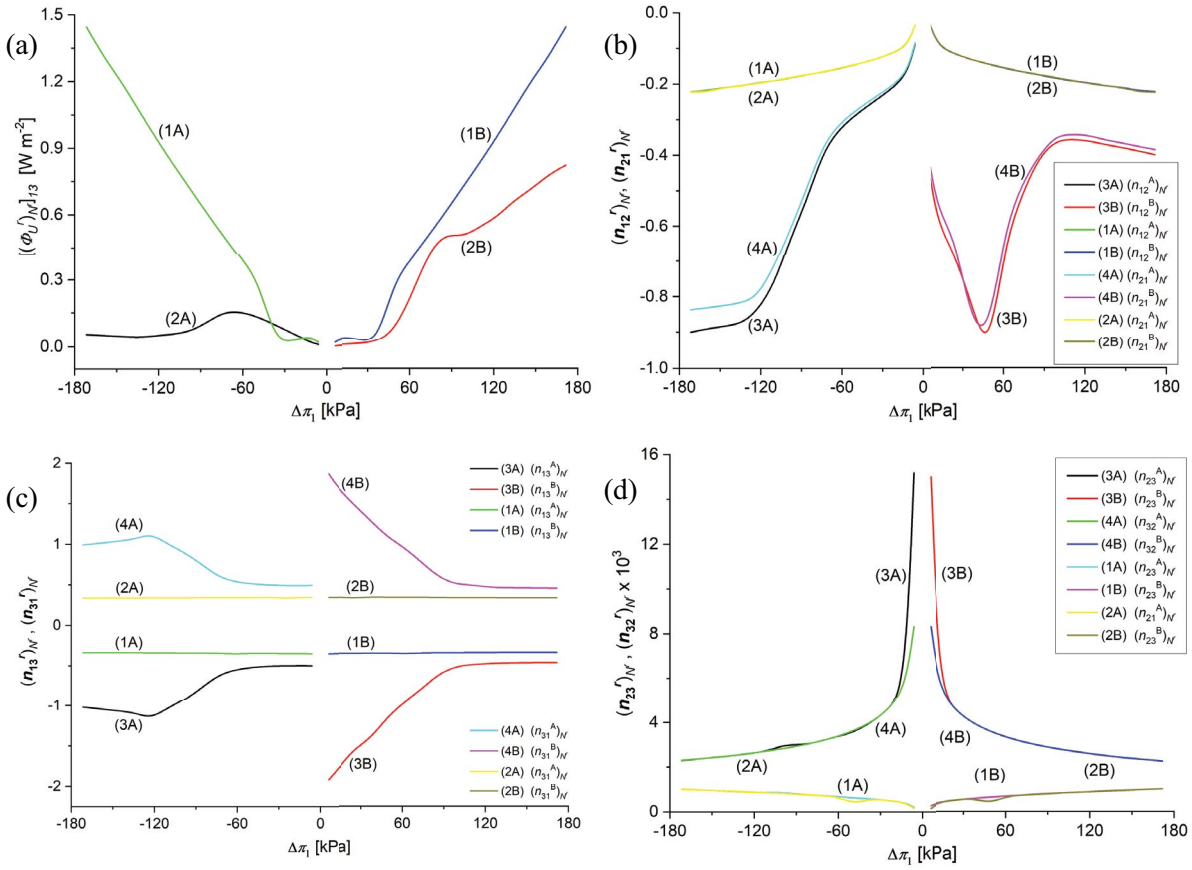

Fig. 6. (a) Total production of *U*-energy $\left[\left(\phi_U^r\right)_{N^r}\right]_{13}$ as a function of osmotic pressure difference of glucose ($\Delta\pi_1$) with a constant osmotic pressure of ethanol ($\Delta\pi_2$ = 490.3 kPa) and ΔP = 0. The coefficients $\left(n_{ij}^r\right)_{N^r}$ as functions of glucose osmotic pressure difference ($\Delta\pi_1$) for $\Delta\pi_2$ = 490.2 kPa and *i*, *j* = {1, 2 or 2, 1 (b), 1, 3 or 3, 1 (b) and 2, 3 or 3, 2 (d)} and *r* = A, B.

on both $\Delta\pi_1$ and configuration of the membrane system, as is shown in curves 3A and 3B. Curve 3A shows that as $\Delta\pi_1$ increases, the value of $\left(n_{13}^A\right)_{N^r}$ initially decreases from –1.02 to a minimal value (–1.16 for $\Delta\pi_1 > -122.5$ kPa) and then increases to –0.5 for $\Delta\pi_1 > -36.8$ kPa. On the other hand, curve 3B shows that as $\Delta\pi_1$ increases, the value of $\left(n_{13}^B\right)_{N^r}$ increases nonlinearly from –1.92 to –0.46.

Similarly, the values of the coefficients $\left(n_{13}^r\right)_{N^r}$ and $\left(n_{31}^r\right)_{N^r}$ depend nonlinearly on both $\Delta\pi_1$ and the configuration of the membrane system, as is illustrated by the curves 4A and 4B. Curve 4A shows that as $\Delta\pi_1$ increases, the value of $\left(n_{13}^A\right)_{N^r}$ initially increases from 0.99 to a maximum value (1.134 for $\Delta\pi_1 > -122.5$ kPa) and then decreases to 0.5 for $\Delta\pi_1 > -36.8$ kPa. For $\Delta\pi_1 \geq -36.8$ kPa $\left(n_{13}^A\right)_{N^r}$ is constant. On the other hand, from curve 4B it can be seen that as $\Delta\pi_1$ increases, the value of $\left(n_{13}^B\right)_{N^r}$ decreases nonlinearly from 1.87 to 0.46. In addition, curves 1A, 2A and 1B, 2B are symmetrical about the horizontal axis passing through the point $\left(n_{13}^r\right)_{N^r} = \left(n_{31}^r\right)_{N^r} = 0$ and vertical axis passing through the point $\Delta\pi_1$ = 0. On the other hand, curves 3A, 4A and 3B, 4B are symmetrical with respect to the horizontal axis passing through the point $\left(n_{13}^r\right)_{N^r} = \left(n_{31}^r\right)_{N^r} = 0$ and asymmetrical with respect to the vertical axis passing through the point $\Delta\pi_1 = 0$.

Fig. 6d shows the dependencies $\left(n_{23}^r\right)_{N^r} = f(\Delta\pi_1)$ and $\left(n_{32}^r\right)_{N^r} = f(\Delta\pi_1)$ for $\Delta\pi_2$ = 490.2 kPa (*r* = A, B), respectively. Curves 1A, 1B, 2A and 2B illustrate these dependencies for homogeneous solutions. Curves 1A and 2A are symmetrical about the vertical axis passing through the point $\Delta\pi_1$ = 0. For concentration polarization conditions, the values of the coefficients $\left(n_{23}^r\right)_{N^r}$ and $\left(n_{32}^r\right)_{N^r}$ are nonlinearly dependent on $\Delta\pi_1$ and do not depend on the configuration of the membrane system, as is illustrated by curves 3A, 3B, 4A and 4B. In addition, all graphs are pairwise symmetric, with respect to the vertical axis passing through the point $\Delta\pi_1 = 0$.

From the results shown in Fig. 6b–d, it can be seen that for homogeneous solutions $\left(n_{12}^r\right)_{N^r} = \left(n_{21}^r\right)_{N^r} < 0$, $\left(n_{13}^r\right)_{N^r} = \left(n_{31}^r\right)_{N^r} < 0$ and $\left(n_{23}^r\right)_{N^r} = \left(n_{32}^r\right)_{N^r} > 0$. If $\left(n_{12}^r\right)_{N^r} < 0$, then as the stimulus ($\Delta P - \Delta\pi_1 - \Delta\pi_2$) of one process increases, the flux J_{s1}^r of the process coupled to it decreases. Similarly, if $\left(n_{13}^r\right)_{N^r} < 0$, then as the value of stimulus ($\Delta P - \Delta\pi_1 - \Delta\pi_2$) increases, the flux J_{s2}^r of the process coupled with it decreases, etc. On the other hand, if $\left(n_{23}^r\right)_{N^r} > 0$, then the coupling of the processes under consideration leads to an increase in fluxes (the values of fluxes increase with increase of suitable stimuli).

For concentration polarization conditions of solutions $\left(n_{12}^r\right)_{N^r} \neq \left(n_{21}^r\right)_{N^r} < 0$, $\left(n_{13}^r\right)_{N^r} \neq \left(n_{31}^r\right)_{N^r}$ and $\left(n_{13}^r\right)_{N^r} < 0$ and $\left(n_{31}^r\right)_{N^r} > 0$, $\left(n_{23}^r\right)_{N^r} \neq \left(n_{32}^r\right)_{N^r} > 0$. If $\left(n_{12}^r\right)_{N^r} < 0$, then as the value of the stimulus $(\Delta P - \Delta\pi_1 - \Delta\pi_2)$ of one process increases, the flux J_{s1}^r of the process coupled to it decreases. Similarly, if $\left(n_{13}^r\right)_{N^r} < 0$, then as the stimulus $(\Delta P - \Delta\pi_1 - \Delta\pi_2)$ increases, the flux J_{s2}^r of the process coupled with it decreases. On the other hand, if $\left(n_{31}^r\right)_{N^r} > 0$ and $\left(n_{23}^r\right)_{N^r} > 0$, then the coupling of the processes under consideration leads to an increase in fluxes.

The results presented in Fig. 6c show that for concentration polarization conditions (curves 3A, 3B, 4A and 4B) the relations $-1.163 \le \left(n_{13}^A\right)_{N^r} \le -0.5$, $-1.917 \le \left(n_{13}^B\right)_{N^r} \le -0.463$, $0.493 \le \left(n_{31}^A\right)_{N^r} \le 1.134$, $0.46 \le \left(n_{31}^B\right)_{N^r} \le 1.87$ are fulfilled. This means that for concentration polarization conditions Caplan's relations are not satisfied.

3.6. Osmotic pressure dependencies of the Peusner's coupling parameter $\left(Q_{ij}^r\right)_{N^r}$

The $\left(Q_{ij}^r\right)_{N^r}$ parameter can be calculated using Eq. (36) and dependencies $N_{ij}^r = f(\Delta\pi_1)$ for $\Delta\pi_2 = 490.2$ kPa presented in Figs. 2a–d and 3a–c.

$$\left(Q_{ij}^r\right)_{N^r} = \frac{2N_{ij}^r N_{ji}^r}{4N_{ii}^r N_j^r - 2N_{ij}^r N_{ji}^r}, \left(i,j \in \{1,2,3\}, r = A,B\right) \tag{35}$$

Fig. 7a shows the dependence $\left(Q_{12}^r\right)_{N^r}$ and $\left(Q_{13}^r\right)_{N^r}$ on $\Delta\pi_1$ for homogeneous solutions, the values of these coefficients do not dependent on the glucose concentration and configuration of the membrane system. The values of these coefficients are $\left(Q_{12}^A\right)_{N^r} = \left(Q_{12}^B\right)_{N^r} = 0.025$ (Fig. 7a, curves 1A and 1B) and $\left(Q_{13}^A\right)_{N^r} = \left(Q_{13}^B\right)_{N^r} = -0.05$ (Fig. 7a, curves 2A and 2B). For concentration polarization conditions, the coefficients $\left(Q_{12}^r\right)_{N^r}$ and $\left(Q_{13}^r\right)_{N^r}$ depend nonlinearly on both $\Delta\pi_1$ and configuration of the membrane system, as is shown in curves 3A, 3B, 4A and 4B.

Curve 3A shows that as $\Delta\pi_1$ increases, the value of $\left(Q_{12}^A\right)_{N^r}$ initially decreases from 0.6 to a minimal value 0.004. On the other hand, curve 4A shows that as $\Delta\pi_1$ increases, the value of $\left(Q_{12}^A\right)_{N^r}$ decreases from –0.34 to minimal value –0.4 (for $\Delta\pi_1$ = –110.29 kPa). For $\Delta\pi_1 > -110.29$ kPa $\left(Q_{12}^A\right)_{N^r}$ increases to maximal value –0.11. Similarly, the value of the coefficients $\left(Q_{12}^B\right)_{N^r}$ and $\left(Q_{13}^B\right)_{N^r}$ depend nonlinearly on $\Delta\pi_1$ and on configuration of the membrane system, as is illustrated by curves 4A and 4B. Curve 4A shows that as $\Delta\pi_1$ increases, the value of $\left(Q_{13}^A\right)_{N^r}$ initially decreases from –0.34 to minimal value –0.4 (for $\Delta\pi_1$ = –122.5 kPa) and then increases to value –0.11 (for $\Delta\pi_1 > -36.8$ kPa). For $\Delta\pi_1 \ge -36.8$ kPa $\left(Q_{13}^A\right)_{N^r}$ is constants. On the other hand, from the curve 4B it can be seen that as $\Delta\pi_1$ increases, the value of $\left(Q_{13}^B\right)_{N^r}$ decreases nonlinearly from –0.64 to –0.1. In addition, curves 1A and 2A and 1B and 2B are symmetrical with respect to the horizontal axis passing through the point $\left(Q_{12}^r\right)_{N^r} = \left(n_{13}^r\right)_{N^r} = 0$ and the vertical axis passing through the point $\Delta\pi_1 = 0$. On the other hand, curves 3A and 4A and 3B and 4B are symmetrical with respect to the horizontal axis passing through the point $\left(Q_{12}^r\right)_{N^r} = \left(Q_{13}^r\right)_{N^r} = 0$ and asymmetrical with respect to the vertical axis passing through the point $\Delta\pi_1 = 0$.

Curves 1A and 1B shown in Fig. 7b illustrate the nonlinear dependence $\left(Q_{23}^r\right)_{N^r} = f(\Delta\pi_1)$ for $\Delta\pi_2$ = 490.2 kPa, for homogeneous solutions and configurations A and B of the membrane system. The aforementioned relations for homogeneous solutions are symmetric curves independent on the configuration of the membrane system.

For concentration polarization conditions, the dependencies $\left(Q_{23}^r\right)_{N^r} = f(\Delta\pi_1)$ for $\Delta\pi_2$ = 490.2 kPa are illustrated by straight line 2A and nonlinear curve 2B. This means that graphs 2A and 2B are dependent on the configuration of the membrane system and are asymmetric with respect to the vertical line passing through the point $\Delta\pi_1 = 0$. The coupling parameters satisfy the relations $0 \le \left(Q_{12}^r\right)_{N^r} \le 0.611$, $-0.642 \le \left(Q_{13}^r\right)_{N^r} \le -0.06$, and $0.641 \times 10^{-6} \le \left(Q_{12}^r\right)_{N^r} \le 2.085 \times 10^{-6}$. Peusner's coupling parameter $\left(Q_{ij}^r\right)_{N^r}$ can be rearranged by Caplan's

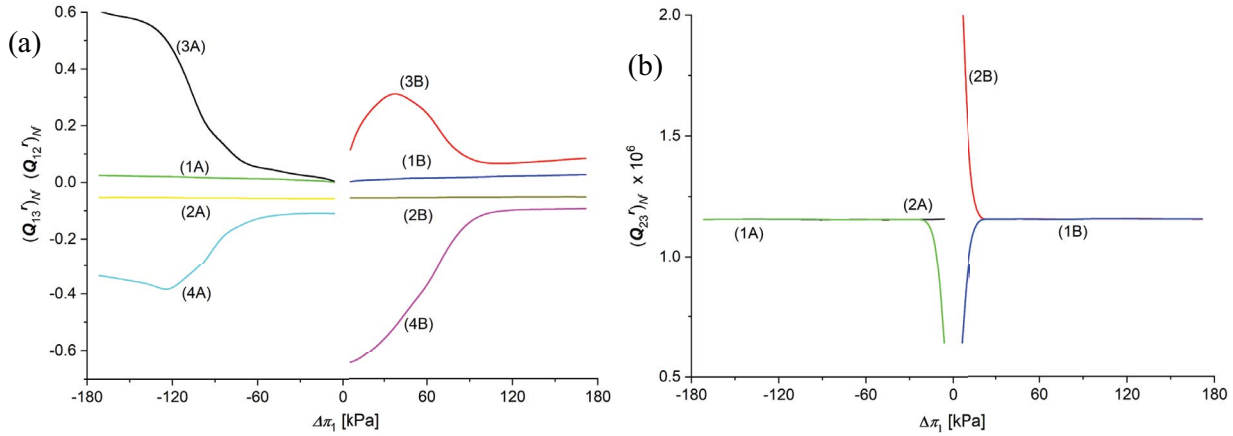

Fig. 7. Coefficients $\left(Q_{ij}^r\right)_{N^r}$ (r = A, B) as functions of glucose osmotic pressure difference ($\Delta\pi_1$) for $\Delta\pi_2$ = 490.2 kPa and (i, j) = {(1, 3) and (1, 2) (a) and (2, 3) (b)}.

coupling coefficients (n^r_{ij}, n^r_{ji}). Considering Eq. (34) in Eq. (35), we get:

$$\left(Q^r_{ij}\right)_{N^r} = \frac{n^r_{ij}n^r_{ji}}{2-n^r_{ij}n^r_{ji}}, \left(i \neq j \in \{1,2,3\}; r = A,B; n^r_{ij}n^r_{ji} \neq 2\right) \quad (36)$$

Considering the results of the calculations shown in Fig. 6b–d in Eq. (36), we get the following relation $-\infty \leq \left(Q^r_{ij}\right)_{N^r} \leq +\infty$.

3.7. Osmotic pressure dependencies of χ_{ij}

The values of the χ_{ij} and χ_{det} coefficients:

$$\chi_{ij} = \frac{N^A_{ij(ji)} - N^B_{ij(ji)}}{N_{ij(ji)}}, \left(i,j \in \{1,2,3\}\right) \quad (37)$$

$$\chi_{det} = \frac{N^A_{det} - N^B_{det}}{N_{det}} \quad (38)$$

can be calculated using the formulas and dependencies $N^r_{ij} = f(\Delta\pi_1)$ for $\Delta\pi_2$ = 490.2 kPa and $N^r_{det} = f(\Delta\pi_1)$ for $\Delta\pi_2$ = 490.2 kPa presented in Figs. 2a–d and 3a–d. The calculated coefficients χ_{ij} and χ_{det} are shown in Fig. 8a–c.

Fig. 8a shows the dependence $\chi_{11} = f(\Delta\pi_1)$ for $\Delta\pi_2$ = 490.2 kPa (curves 1A and 1B) $\chi_{33} = f(\Delta\pi_1)$ for $\Delta\pi_2$ = 490.2 kPa (curves 2A and 2B) and $\chi_{det} = f(\Delta\pi_1)$ for $\Delta\pi_2$ = 490.2 kPa (curves 3A and 3B). From this figure it results that $\chi_{11} = \chi_{33} = \chi_{det} = 0$ for $\Delta\pi_1$ = 78.75 kPa. In contrast, $\chi_{11} > 0$ and $\chi_{det} > 0$ for $\Delta\pi_1 < -78.75$ kPa and for $\Delta\pi_1 > 78.75$ kPa. Besides, $\chi_{33} > 0$, for $\Delta\pi_1 > -78.75$ kPa and for $\Delta\pi_1 < 78.75$ kPa. On the other hand, $\chi_{11} < 0$, $\chi_{det} < 0$ for $\Delta\pi_1 > -78.75$ kPa and for $\Delta\pi_1 < 78.75$ kPa and $\chi_{33} < 0$ for $\Delta\pi_1 < -78.75$ kPa and for $\Delta\pi_1 > 78.75$ kPa.

Fig. 8b shows the dependence $\chi_{12} = f(\Delta\pi_1)$ (curves 1A and 1B), $\chi_{21} = f(\Delta\pi_1)$ (curves 2A and 2B) and $\chi_{22} = f(\Delta\pi_1)$ (curves 3A and 3B) for $\Delta\pi_2$ = 490.2 kPa. This figure shows that $\chi_{12} = \chi_{21} = 0$ for $\Delta\pi_1$ = 78.75 kPa. In turn $\chi_{11} > 0$, $\chi_{33} > 0$ and $\chi_{det} > 0$ for $\Delta\pi_1 < -78.75$ kPa and for $\Delta\pi_1 > 78.75$ kPa. On the other hand, $\chi_{11} < 0$, $\chi_{33} < 0$ and $\chi_{det} < 0$ for $\Delta\pi_1 > -78.75$ kPa and for $\Delta\pi_1 < 78.75$ kPa.

Fig. 8c shows the dependence $\chi_{13} = f(\Delta\pi_1)$ (curves 1A and 1B) and $\chi_{31} = f(\Delta\pi_1)$ (curves 2A and 2B) for $\Delta\pi_2$ = 490.2 kPa. This figure shows that $\chi_{13} = 0$, for $\Delta\pi_1$ = 78.75 kPa. In contrast, $\chi_{13} > 0$ for $\Delta\pi_1 < -78.75$ kPa and for $\Delta\pi_1 > 78.75$ kPa. Whereas $\chi_{31} > 0$, for $\Delta\pi_1 < -97.5$ kPa and for $\Delta\pi_1 > 97.5$ kPa. In contrast, $\chi_{33} < 0$, for $\Delta\pi_1 > -97.5$ kPa and for $\Delta\pi_1 < 97.5$ kPa. It should be noted that $\chi_{23} = \chi_{32} = 0$.

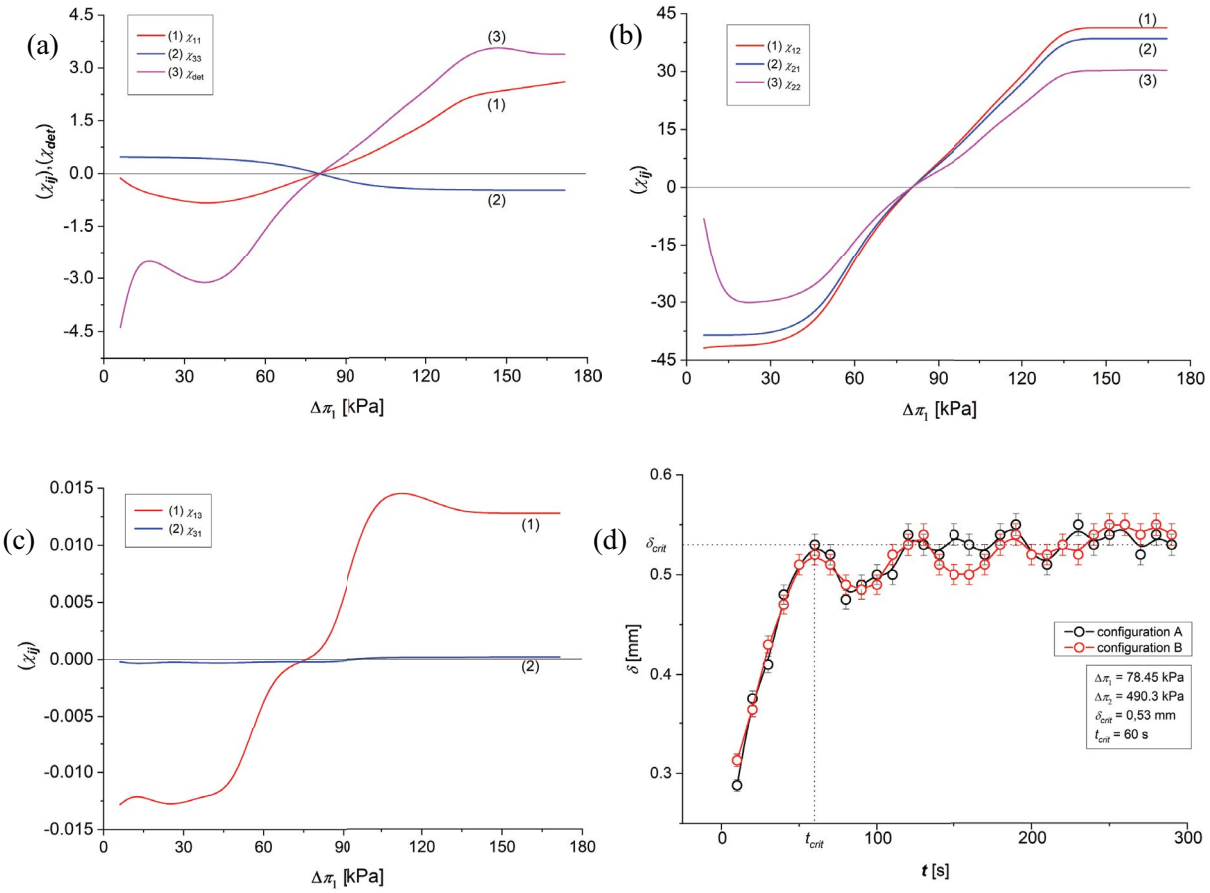

Fig. 8. Coefficients: $\chi_{ij} = f(\Delta\pi_1)$ and $\chi_{det} = f(\Delta\pi_2)$ as functions of glucose osmotic pressure difference ($\Delta\pi_1$) for $\Delta\pi_2$ = 490.2 kPa and (i, j) = {(1, 1), (3, 3) and det (a), (1, 2), (2, 1) and (2, 2) (b), (1, 3) and (3, 1) (c)}. Thickness of CBLs as a function of time of CBLs rebuilding $\delta = f(t)$ (d).

Fig. 8d shows the temporal dependence of CBL thickness (δ) for $\Delta\pi_1$ = 78.45 kPa and $\Delta\pi_2$ = 490.3 kPa. Experimental studies were carried out using the measurement set described in the previous papers [7,55–57]. This measurement set consisted of a membrane system, a Mach–Zehnder interferometer, a TV-CCD camera, and a computerized data acquisition system. Interferograms, obtained for the Nephrophan membrane, which was located in a horizontal plane and separated glucose solutions in an aqueous ethanol solution were presented in the paper [47]. The methodology for calculating $\delta = f(t)$ on the basis of data obtained by the interferometric method is presented in articles [7,55–57]. Fig. 8d shows that the dependencies $\delta = f(t)$ for $t < t_{crit}$ and configurations A and B are identical (t_{crit} = 50 s, d_{crit} = 0.53 mm). For $t > t_{crit}$, d fluctuates around the critical value. Fluctuations are a manifestation of free convection in near-membrane areas [44,47].

3.8. Dependencies between Peusner coefficients (N_{ij}^r, N_{det}^r) and Péclet coefficients ($\wp_{vk}^r$, $\wp_{ak}^r$)

The classic Péclet coefficient ($\wp$) known from the literature [50,51] is expressed by the ratio of the rate of advection and the rate of diffusion. This ratio can be represented by the equation $\wp = (1 - \sigma)\ell^{-1}$, where σ is the dimensionless reflection coefficient and ℓ is the transmittance coefficient of the solute expressed in units m·s^{-1}. Thus, $\wp$ is expressed in s·m^{-1}. The product of $\wp$ and J_v is called the Péclet number (Pe), and it is a dimensionless quantity. Due to the fact that $\ell = \omega RT$, where ω – membrane permeability coefficient, we can write $\wp = (1 - \sigma)(\omega RT)^{-1}$. By entering the following notations:

$$\kappa_{v1}^r \equiv -\frac{1-\sigma_{v1}\zeta_{v1}^r}{\omega_{11}\zeta_{s11}^r} = -N_{12}^r \tag{39}$$

$$\kappa_{a1}^r \equiv -\frac{1-\sigma_{a1}\zeta_{a1}^r}{\omega_{11}\zeta_{s11}^r} = -N_{21}^r \tag{40}$$

$$\kappa_{v2}^r \equiv \frac{1-\sigma_{v2}\zeta_{v2}^r}{\omega_{11}\zeta_{s11}^r} \tag{41}$$

$$\kappa_{a2}^r \equiv \frac{1-\sigma_{a2}\zeta_{a2}^r}{\omega_{11}\zeta_{s11}^s} \tag{42}$$

we can express the Péclet coefficients $\wp_{v1}^r$, $\wp_{v2}^r$, $\wp_{a1}^r$ and $\wp_{a2}^r$ for concentration polarization conditions by the equations.

$$\wp_{v1}^r = -\frac{1-\sigma_{v1}\zeta_{v1}^r}{\omega_{11}\zeta_{s1}^r RT\bar{C}_1} = -\frac{N_{12}^r}{RT\bar{C}_1} = \frac{\kappa_{v1}^r}{RT\bar{C}_1} \tag{43}$$

$$\wp_{a1}^r = -\frac{1-\sigma_{a1}\zeta_{a1}^r}{\omega_{11}\zeta_{s11}^r RT} = -\frac{N_{21}^r}{RT} = \frac{\kappa_{a1}^r}{RT} \tag{44}$$

$$\wp_{v2}^r = -\frac{\left(1-\sigma_{v2}\zeta_{v2}^r\right)D_2}{\omega_{11}\zeta_{s11}^r\delta} = \frac{\kappa_{v2}^r D_2}{\delta} \tag{45}$$

$$\wp_{a2}^r = -\frac{1-\sigma_{a2}\zeta_{a2}^r}{\omega_{11}\zeta_{s11}^r RT} = \frac{\kappa_{a2}^r}{RT} \tag{46}$$

The unit of $\wp_{v1}^r$ is s·m^2·mol^{-1}, $\wp_{a1}^r$ – s·m^{-1}, $\wp_{v2}^r$ – mol·N^{-1}·m^{-1} and $\wp_{a2}^r$ – s·m^{-1}.

Using Eqs. (43)–(46), Eqs. (14)–(17), (20) and (24) can be written in the following forms:

$$N_{11}^r = \frac{1}{L_p\zeta_p^r} + \bar{C}_1^2\omega_{11}\zeta_{s11}^r\left(RT\right)^2\wp_{v1}^r\wp_{a1}^r \tag{47}$$

$$N_{12}^r = -\frac{1-\sigma_{v1}\zeta_{v1}^r}{\omega_{11}\zeta_{s11}^r} = -\bar{C}_1 RT\wp_{v1}^r \tag{48}$$

$$N_{13}^r = \bar{C}_2 RT\left[\bar{C}_1\omega_{12}\zeta_{s12}^r\wp_{v1}^r - \frac{\omega_{11}\zeta_{s11}^r\delta}{D_2}\wp_{v2}^r\right] \tag{49}$$

$$N_{21}^r = -\frac{1-\sigma_{a1}\zeta_{a1}^r}{\omega_{11}\zeta_{s11}^r} = -RT\wp_{a1}^r \tag{50}$$

$$N_{31}^r = RT\left[\bar{C}_2\omega_{11}\zeta_{s11}^r\wp_{a2}^r - \bar{C}_1\omega_{21}\zeta_{s21}^r\wp_{a1}^r\right] \tag{51}$$

$$\det\left[N^r\right] = N_{det}^r = \frac{\bar{C}_2}{\bar{C}_1}\left[\frac{\omega_{22}\zeta_{s22}^r}{L_p\zeta_p^r\omega_{11}\zeta_{s11}^r} + \frac{\bar{C}_2\left(RT\right)^2\delta\omega_{11}\zeta_{s11}^r\wp_{a2}^r\wp_{v2}^r}{D_2}\right] \tag{52}$$

Using coefficients $\wp_{v1}^r$, $\wp_{v2}^r$, $\wp_{a1}^r$ or $\wp_{a2}^r$, we can write the equations for modified Péclet numbers for fluxes (J_1^r, J_v^r) and for thermodynamic forces ($\Delta\pi_2/\bar{C}_2$).

$$\left(\mathrm{Pe}\right)_{v1}^r = \wp_{v1}^r J_1^r \tag{53}$$

$$\left(\mathrm{Pe}\right)_{a1}^r = \wp_{a1}^r J_v^r \tag{54}$$

$$\left(\mathrm{Pe}\right)_{v2}^r = \wp_{v2}^r\left(\frac{\Delta\pi_2}{\bar{C}_2}\right) \tag{55}$$

$$\left(\mathrm{Pe}\right)_{a2}^r = \wp_{a2}^r J_v^r \tag{56}$$

3.9. Dependences between $\left(e_{ij}^r\right)_{N^r}$ coefficients, n_{ij}^r, n_{ji}^r coefficients and Q_{ij}^r

Using Eqs. (34) and (35), Eqs. (29), (30) and (34) can be converted to the form:

$$\left[\left(e_{ij}^r\right)_{N^r}\right]_{max} = \frac{n_{ij}^r n_{ji}^r}{\left(1+\sqrt{1-n_{ij}^r}h_{ji}^r\right)^2} = \frac{2\left(Q_{ij}^r\right)_{N^r}}{\left(1+\left(Q_{ij}^r\right)_{N^r}\right)\left(1+\sqrt{1-\frac{2\left(Q_{ij}^r\right)_{N^r}}{1+\left(Q_{ij}^r\right)_{N^r}}}\right)^2} \tag{57}$$

The values of the coefficients $\left(e_{ij}^{r}\right)_{N^r}$ are limited by the relation $0 \le \left(e_{ij}^{r}\right)_{N^r} \le +1$. Taking into account Eqs. (57) in (28) we get:

$$\left[\left(\phi_F^r\right)_{N^r}\right]_{ij} = \frac{n_{ij}^r n_{ji}^r}{\left(1+\sqrt{1-n_{ij}^r n_{ji}^r}\right)^2 - n_{ij}^r n_{ji}^r}\left(\phi_S^r\right)_{N^r} = \frac{2\left(Q_{ij}^r\right)_{N^r}}{\left(1+\left(Q_{ij}^r\right)_{N^r}\right)\left(1+\sqrt{\frac{1-\left(Q_{ij}^r\right)_{N^r}}{1+\left(Q_{ij}^r\right)_{N^r}}}\right)^2 - 2\left(Q_{ij}^r\right)_{N^r}}\left(Q_S^r\right)_{N^r} \tag{58}$$

To obtain the equation for $\left(\phi_U^r\right)_{N^r}$ it is necessary to include Eq. (31) in Eq. (29).

Using Eqs. (25) and (58) can be transformed to the form:

$$\left[\left(\phi_U^r\right)_{N^r}\right]_{ij} = \left[1 - \frac{n_{ij}^r n_{ji}^r}{\left(1+\sqrt{1-n_{ij}^r n_{ji}^r}\right)^2}\right]^{-1}\left(\phi_S^r\right)_{N^r} = \left[1 - \frac{2\left(Q_{ij}^r\right)_{N^r}}{\left(1+\left(Q_{ij}^r\right)_{N^r}\right)\left(1+\sqrt{\frac{1-\left(Q_{ij}^r\right)_{N^r}}{1+\left(Q_{ij}^r\right)_{N^r}}}\right)^2}\right]^{-1}\left(\phi_S^r\right)_{N^r} \tag{59}$$

Most of the curves illustrating the dependencies $N_{ij}^r = f(\Delta\pi_1)$ and $N_{\text{det}}^r = f(\Delta\pi_1)$ for $\Delta\pi_2 = 490.2$ kPa ($i, j \in \{1, 2, 3\}$, r = A, B) shown in Figs. 2 and 3 for concentration polarization conditions are nonlinear and depend on $\Delta\pi_1$ and membrane system configuration. This dependence makes the mentioned curves asymmetric with respect to the vertical axis passing through the point $\Delta\pi_1 = 0$. Moreover, the nonlinearities of these dependencies are reflected in the curves, which illustrate the dependencies of coefficients $\left(\varphi_S^r\right)_{N^r}$, $\left[\left(e_{ij}^r\right)_{N^r}\right]_{\max}$, $\left[\left(\phi_F^r\right)_{N^r}\right]_{ij}$, $\left[\left(\phi_U^r\right)_{N^r}\right]_{ij} n_{ij}^r$, $\left(Q_{ij}^r\right)_{N^r}$ and $\left(\chi_{ij}\right)$ on $\Delta\pi_1$ and membrane system configurations, shown in Figs. 4–8.

The curves shown in Fig. 8a–c facilitate the evaluation of the concentration Rayleigh number R_C^r), which controls the process of transition of the system from the convection-free to the convective state or vice versa. The most important is the critical value of this number $(R_C^r)_{\text{crit}}$, which acts as a bifurcation point. To demonstrate the usefulness of the coefficient χ_{ij} to determine the critical value of the concentration Rayleigh number $(R_C^r)_{\text{crit}}$, let us consider the relationship $\chi_{ij} = f(\Delta\pi_1)$ for $\Delta\pi_2 = 490.2$ kPa ($i, j \in \{1, 2, 3\}$ shown in Fig. 8a–c and the equation representing the concentration Rayleigh number for membrane transport processes of solutions consisting of water and two solutes proposed in the papers [44,54].

$$R_C^r = \frac{g\omega_{11}}{D_1\left(D_1 + 2RT\omega_{11}\delta\right)\rho_l \nu_l}\left[\left(\frac{\partial\rho}{\partial C_1}\right)\Delta\pi_1 + \frac{\omega_{22}\left(D_1 + 2RT\omega_{12}\delta\right)}{\omega_{11}\left(D_2 + 2RT\omega_{22}\delta\right)}\left(\frac{\partial\rho}{\partial C_2}\right)\Delta\pi_2\right]\delta^4 \tag{60}$$

where g – earth acceleration, D_1, D_2 – diffusion coefficients of the first and second solute, respectively, R – universal gas constant, T – absolute temperature, ω_{11}, ω_{22} – permeability coefficients of the first and second solute, respectively, ρ_l – density of water, v_l – viscosity coefficient of water, $\Delta\pi_1$, $\Delta\pi_2$ – osmotic pressure differences, $\partial\rho/\partial C_1$, $\partial\rho/\partial C_2$ – change in density due to change in concentration of the first component and/or the second component, respectively, δ – thickness of concentration boundary layer. To calculate the critical value of R_C^r by means of Eq. (61), we will consider the following data: $g = 9.81$ m·s^{-2}, $D_1 = 0.69 \times 10^{-9}$ m^2·s^{-1}, $D_2 = 1.07 \times 10^{-9}$ m^2·s^{-1}, $R = 8.31$ J·mol^{-1}·K^{-1}, $T = 295$ K, $\omega_{11} = 0.8 \times 10^{-9}$ mol·N^{-1}·s^{-1}, $\omega_{22} = 1.43 \times 10^{-9}$ mol·N^{-1}·s^{-1}, $\rho_l = 998$ kg·m^{-3}, $v_l = 1.01 \times 10^{-6}$ m^2·s^{-1}, $\partial\rho/\partial C_1 = 0.06$ kg·mol^{-1}, $\partial\rho/\partial C_2 = -0.009$ kg·mol^{-1} and $\Delta\pi_2 = 490.2$ kPa. In addition, from Fig. 8 we read the value of $\Delta\pi_1 = \pm 78.75$ kPa (e.g., for $\chi_{12} = 0$) and from Fig. 8d we read the critical value of concentration boundary layer thickness $\delta_{\text{crit}} = 0.53$ mm. The calculated critical value of the concentration Rayleigh number is $(R_C^r)_{\text{crit}} = 414.2$. It should be mentioned that the relationship $\delta = f(t)$ was determined by laser interferometry.

4. Conclusions

Research has shown that:

- The description of the transport of ternary non-electrolyte solutions through a horizontally oriented membrane using the N^r version of the Kedem–Katchalsky–Peusner equations introduces nine Peusner coefficients N_{ij}^r ($i, j \in \{1, 2, 3\}$, r = A, B) and the coefficient N_{det}^r, which is equal to the determinant of the matrix $[N^r]$.
- For Nephrophan membrane separating solutions of glucose in aqueous ethanol solutions in concentration polarization conditions, the values of N_{ij}^r ($i, j \in \{1, 2, 3\}$, r = A, B) and N_{det}^r coefficients are nonlinearly dependent on glucose osmotic pressure difference $\Delta\pi_1$ ($\Delta\pi_2 = 490.2$ kPa) and membrane system configuration. The non-diagonal coefficients do not satisfy the alternation relation which means that $N_{12}^r \ne N_{21}^r$, $N_{13}^r \ne N_{31}^r$ and $N_{23}^r \ne N_{32}^r$.
- For homogeneous solutions, the coefficients N_{ij}^r ($i, j \in \{1, 2, 3\}$, r = A, B) and N_{det}^r do not depend on the configuration of the membrane system and the coefficients N_{12}^r, N_{21}^r, N_{13}^r and N_{33}^r do not depend on $\Delta\pi_1$.
- The concentration dependencies of the coefficients χ_{ij} and χ_{det} can be used to determine the direction of natural convection: for $\chi_{ij} < 0$ or $\chi_{\text{det}} < 0$, natural convection is vertically upward, and for $\chi_{ij} > 0$ or $\chi_{\text{det}} > 0$, it is vertically downward. $\chi_{ij} = 0$, $\chi_{\text{det}} = 0$, refer to non-convective state.
- The N^r form of the equations of the Kedem–Katchalsky–Peusner model is a useful tool for calculating the dissipated energy (S-energy), coefficients N_{ij}^r and the fluxes J_v^r, J_k^r, used for the analysis of internal energy conversion (U-energy). The aim of presented method of energy conversion analysis in membrane systems is to calculate the free energy (F-energy) $\left[\left(\phi_F^r\right)_{N^r}\right]_{ij}$ based on an expression containing the production of S-energy $\left(\varphi_S^r\right)_{N^r}$ and energy conversion efficiency coefficient $\left[\left(e_{ij}^r\right)_{N^r}\right]_{\max}$.

- The energy conversion efficiency $\left[\left(e_{ij}^{r}\right)_{N^r}\right]_{\max}$ can be calculated from the N_{ij}^{r} coefficients. The largest value of *F*-energy appears when the equation for $\left[\left(\phi_{F}^{r}\right)_{N^r}\right]_{ij}$ includes the coefficient $\left[\left(e_{13}^{r}\right)_{N^r}\right]_{\max}$.
- These results may be useful for studying the transport properties of new polymeric membranes modified with nanoparticles, providing an increase in hydraulic performance while maintaining high separation efficiency and controlling pore blockage phenomena.

Acknowledgements

The scientific research was funded both by the statute subvention of Czestochowa University of Technology, Jan Dlugosz University in Czestochowa, Silesian University of Technology in Gliwice, Silesia University in Katowice and Silesian Medical University in Katowice.

Symbols

L_{ij}^{r}, R_{ij}^{r}	—	Symmetric Peusner's coefficients for non-homogeneous solutions for binary solutions (i, $j \in \{1, 2\}$, r = A, B)
H_{ij}^{r}, P_{ij}^{r}	—	Hybrid Peusner's coefficients for non-homogeneous solutions for binary solutions (i, $j \in \{1, 2\}$, r = A, B)
L_{ij}^{r}, R_{ij}^{r}	—	Symmetric Peusner's coefficients for non-homogeneous solutions for ternary solutions (i, $j \in \{1, 2, 3\}$, r = A, B)
H_{ij}^{r}, P_{ij}^{r}	—	Hybrid Peusner's coefficients for non-homogeneous solutions for binary for ternary solutions (i, $j \in \{1, 2, 3\}$, r = A, B)
H_{ij}^{r}, K_{ij}^{r} N_{ij}^{r}, S_{ij}^{r} W_{ij}^{r}, P_{ij}^{r}		
L_p	—	Hydraulic permeability coefficient, $m^3 \cdot N^{-1} \cdot s^{-1}$
J_v^r	—	Volume flux in non-homogeneous conditions, $m \cdot s^{-1}$
J_k^r	—	Solute flux in non-homogeneous conditions, $mol \cdot m^{-2} \cdot s^{-1}$
C_{hk}, C_{lk}	—	Concentrations of solutions in chambers of the membrane system, $mol \cdot m^{-3}$
C_{hk}^{r}, C_{lk}^{r}	—	Concentrations of solutes at interfaces: l_h^r/M and M/l_l^r, $mol \cdot m^{-3}$
$\bar{C}_k$	—	Mean solute concentration in the membrane, $mol \cdot m^{-3}$
l_h^r, l_l^r	—	Concentration boundary layers (CBLs), m
l_h^r/M/l_l^r	—	Complex CBL/M/CBL
RT	—	Product of the gas constant and thermodynamic temperature, $J \cdot mol^{-1}$
P_h, P_l	—	Hydrostatic pressures (h higher and l lower value), Pa
ΔP	—	Hydrostatic pressure difference, Pa
D_k	—	Diffusion coefficient, $m^2 \cdot s^{-1}$
n_{ij}^{r}	—	Degree of coupling for diluted and non-homogeneous solutions
$\left[Q_{ij}^{r}\right]_{N^r}$	—	Peusner's coupling parameter for diluted and non-homogeneous solutions
$\left[\left(e_{ij}^{r}\right)_{N^r}\right]_{\max}$	—	Energy conversion efficiency for diluted and non-homogeneous solutions
$\left(\phi_{S}^{r}\right)_{N^r}$	—	Flux of the *S*-energy, $W \cdot m^{-2}$
$\left[\left(\phi_{F}^{r}\right)_{N^r}\right]_{ij}$	—	Flux of the *F*-energy, $W \cdot m^{-2}$
$\left[\left(\phi_{U}^{r}\right)_{N^r}\right]_{ij}$	—	Flux of the *U*-energy, $W \cdot m^{-2}$
$\left(\chi_{ij}\right)_{N^r}$	—	Convection effect
R_C^r	—	Concentration Rayleigh number
$\wp_{vk}^{r}$, $\wp_{ak}^{r}$	—	Péclet coefficients for concentration polarization conditions. The unit of $\wp_{v1}^{r}$ is $s \cdot m^2 \cdot mol^{-1}$, $\wp_{a1}^{r}$ – $s \cdot m^{-1}$, $\wp_{v2}^{r}$ – $mol \cdot N^{-1} \cdot m^{-1}$ and $\wp_{a2}^{r}$ – $s \cdot m^{-1}$
$(\mathrm{Pe})_{v1}^{r}$, $(\mathrm{Pe})_{a}^{r}1$, $(\mathrm{Pe})_{v}^{r}2$, $(\mathrm{Pe})_{a}^{r}2$	—	Péclet numbers

Greek letters

$\Delta\pi_k$	—	Osmotic pressure difference, Pa
σ_{vk}, σ_{sk}	—	Reflection coefficients
δ_h^r, δ_l^r	—	Thickness of concentration boundary layers in configurations A and B of membrane system, m
ω_{sk}	—	Solute permeability coefficient, $mol \cdot N^{-1} \cdot s^{-1}$
ζ_p^r	—	Hydraulic concentration polarization coefficient
ζ_{vk}^r	—	Osmotic concentration polarization coefficient
ζ_{sk}^r	—	Diffusive concentration polarization coefficient
ζ_{ak}^r	—	Advective concentration polarization coefficient
$\rho_{l'}$, ρ_h	—	Densities of solutions outside of CBLs, $kg \cdot m^{-3}$
$\rho_{l'}^r$, ρ_l^r	—	Densities of solutions at the interfaces: l_h^r/M and M/l_l^r, $kg \cdot m^{-3}$

References

[1] R. Baker, Membrane Technology and Application, John Wiley & Sons, New York, 2012.
[2] S.V. Jadhav, K.V. Marathe, V.K. Rathod, A pilot scale concurrent removal of fluoride, arsenic, sulfate and nitrate by using nanofiltration: competing ion interaction and modelling approach, J. Water Process Eng., 13 (2016) 153–167.
[3] T. Uragami, Science and Technology of Separation Membranes, John Wiley & Sons, Chichester, UK, 2017.
[4] Y. Dermirel, Nonequilibrium Thermodynamics: Transport and Rate Processes in Physical, Chemical and Biological Systems, Elsevier, Amsterdam, 2007.
[5] V. Gerbaud, N. Shcherbakova, S. Da Cunha, A nonequilibrium thermodynamics perspective on nature-inspired chemical engineering processes, Chem. Eng. Res. Des., 154 (2020) 316–330.
[6] S. Raghuvanshi, B. La Prairie, S. Rajagopal, V.G. Yadav, Chapter 11 – Polymeric Nanomaterials for Ocular Drug Delivery, A.K. Bajpai, R.K. Saini, Eds., Advances in Polymeric Nanomaterials for Biomedical Applications: Micro and Nano Technologies, Elsevier, Amsterdam, 2021.
[7] J. Rewak-Soroczynska, P. Sobierajska, S. Targonska, A. Piecuch, L. Grosman, J. Rachuna, S. Wasik, M. Arabski, R. Ogorek, R.J. Wiglusz, New approach to antifungal activity of fluconazole

incorporated into the porous 6-anhydro-α-l-galacto-β-d-galactan structures modified with nanohydroxyapatite for chronic-wound treatments-*in vitro* evaluation, Int. J. Mol. Sci., 22 (2021) 3112, doi: 10.3390/ijms22063112.
[8] D. Rana, T. Matsuura, S. Sourirajan, Physicochemical and Engineering Properties of Food in Membrane Separation Processes, M.A. Rao, S.S.H. Rizvi, A.K. Datta, J. Ahmed, Eds., Engineering Properties of Foods, Taylor & Francis/CRC Press, Boca Raton, FL, 2014, pp. 437–525.
[9] D. Rana, T. Matsuura, State of the art reviews in membrane science and research, J. Membr. Sci. Res., 3 (2017) 118–119.
[10] D. Rana, T. Matsuura, Membrane Transport Models, D.R. Heldman, C.I. Moraru, Eds., Encyclopedia of Agriculture, Food and Biological Engineering, Taylor & Francis, New York, NY, 2010, pp. 1041–1047.
[11] D. Rana, T. Matsuura, M.A. Kassim, A.F. Ismail, Reverse Osmosis Membrane, A.K. Pabby, S.S.H. Rizvi, A.M. Sastre, Eds., Handbook of Membrane Separations: Chemical, Pharmaceutical, Food, and Biotechnological Applications, Taylor & Francis/CRC Press, Boca Raton, FL, 2015, pp. 35–52.
[12] A. Katchalsky, P.F. Curran, Nonequilibrium Thermodynamics in Biophysics, Harvard University Press, Cambridge, MA, USA, 1965.
[13] D. Kondepudi, I. Prigogine, Modern Thermodynamics: From Heat Engines to Dissipative Structures, John Wiley & Sons, Chichester, 2006.
[14] J.G. Wijmans, R.W. Baker, The solution–diffusion model: a review, J. Membr. Sci., 107 (1995) 1–21.
[15] M.A. Al-Obaidi, C. Kara-Zaitri, I.M. Mujtaba, Scope and limitation of the irreversible thermodynamics and the solution diffusion models for the separation of binary and multi-component systems in reverse osmosis process, Comput. Chem. Eng., 100 (2017) 48–79.
[16] K.S. Spiegler, Transport processes in ionic membranes, Trans. Faraday Soc., 54 (1958) 1408–1428.
[17] O. Kedem, A. Katchalsky, A physical interpretation of the phenomenological coefficients of membrane permeability, J. Gen. Physiol., 45 (1961) 143–179.
[18] A. Ślęzak, A frictional interpretation of the phenomenological coefficients of membrane permeability for multicomponent, non-ionic solutions, J. Biol. Phys., 23 (1997) 239–250.
[19] M.H. Friedman, R.A. Meyer, Transport across homoporous and heteroporous membranes in nonideal, nondilute solutions. I. Inequality of reflection coefficients for volume flow and solute flow, Biophys. J., 34 (1981) 535–544.
[20] E.A. Mason, H.K. Lonsdale, Statistical-mechanical theory of membrane transport, J. Membr. Sci., 51 (1990) 1–81.
[21] X. Cheng, P.M. Pinsky, The balance of fluid and osmotic pressures across active biological membranes with application to the corneal endothelium, PLoS One, 10 (2015) e0145422, doi: 10.1371/journal.pone.0145422.
[22] L. Peusner, The Principles of Network Thermodynamics: Theory and Biophysical Applications, Ph.D. Thesis, Harvard University, Cambridge, MA, USA, 1970.
[23] G. Oster, A. Perelson, A. Katchalsky, Network thermodynamics, Nature, 234 (1971) 239–399.
[24] L. Peusner, Hierarchies of irreversible energy conversion systems: a network thermodynamic approach. I. Linear steady state without storage, J. Theor. Biol., 10 (1983) 27–39.
[25] L. Peusner, Hierarchies of irreversible energy conversion systems. II. Network derivation of linear transport equations, J. Theor. Biol., 115 (1985) 319–335.
[26] L. Peusner, Network representation yielding the evolution of Brownian motion with multiple particle interactions, Phys. Rev. A, 32 (1985) 1237–1238.
[27] L. Peusner, D.C. Mikulecky, B. Bunow; S. Roy Caplan, A network thermodynamic approach to Hill and King–Altman reaction–diffusion kinetics, J. Chem. Phys., 83 (1985) 5559–5566.
[28] L. Peusner, Studies in Network Thermodynamics, Elsevier, Amsterdam, 1986.
[29] L. Peusner, Hierarchies of energy conversion processes III. Why are Onsager equations reciprocal? The euclidean geometry of fluctuation–dissipation space, J. Theor. Biol., 122 (1983) 125–155.
[30] L. Peusner, Premetric thermodynamics. A topological graphical model, J. Chem. Soc., Faraday Trans., 81 (1985) 1151–1161.
[31] A. Ślęzak, S. Grzegorczyn, K.M. Batko, Resistance coefficients of polymer membrane with concentration polarization, Transp. Porous Media, 95 (2012) 151–170.
[32] K.M. Batko, I. Ślęzak-Prochazka, S. Grzegorczyn, A. Ślęzak, Membrane transport in concentration polarization conditions: network thermodynamics model equations, J. Porous Media, 17 (2014) 573–586.
[33] I. Ślęzak-Prochazka, K.M. Batko, S. Wąsik, A. Ślęzak, H* Peusner's form of the Kedem–Katchalsky equations for non-homogenous non-electrolyte binary solutions, Transp. Porous Media, 111 (2016) 457–477.
[34] K.M. Batko, I. Ślęzak-Prochazka, A. Ślęzak, Network hybrid form of the Kedem–Katchalsky equations for non-homogenous binary non-electrolyte solutions: evaluation of P_{ij}^* Peusner's tensor coefficients, Transp. Porous Media, 106 (2015) 1–20.
[35] K.M. Batko, A. Ślęzak, Membrane transport of non-electrolyte solutions in concentration polarization conditions: H^r form of the Kedem–Katchalsky–Peusner equations, Int. J. Chem. Eng., 2019 (2019) 5629259, doi: 10.1155/2019/5629259.
[36] M. Kargol, A. Kargol, Mechanistic equations for membrane substance transport and their identity with Kedem–Katchalsky equations, Biophys. Chem., 103 (2003) 117–127.
[37] H.Y. Elmoazzen, J.A.W. Elliot, L.E. McGann, Osmotic transport across cell membranes in nondilute solutions: a new nondilute solute transport equation, Biophys. J., 96 (2009) 2559–2571.
[38] J. Meixner, Thermodynamics of electrical networks and Onsager–Casimir reciprocal relations, J. Math. Phys., 4 (1963) 154–159.
[39] A. Ślęzak, S. Grzegorczyn, K.M. Batko, W.M. Bajdur, M. Włodarczyk-Makuła, M. Applicability of the L^r form of the Kedem–Katchalsky–Peusner equations for membrane transport in water purification technology, Desal. Water Treat., 202 (2020) 48–60.
[40] K.M. Batko, A. Ślęzak, S. Grzegorczyn, W.M. Bajdur, The R^r form of the Kedem–Katchalsky–Peusner model equations for description of the membrane transport in concentration polarization conditions, Entropy, 22 (2020) 857, doi: 10.3390/e22080857.
[41] K. Batko, I. Ślęzak-Prochazka, A. Ślęzak, W.M. Bajdur, M. Makuła-Włodarczyk, Management of energy conversion processes in membrane system, Energies, 15 (2022) 1661, doi: 10.3390/en15051661.
[42] A. Ślęzak, K. Dworecki, I.H. Ślęzak, S. Wąsik, Permeability coefficient model equations of the complex: membrane-concentration boundary layers for ternary non-electrolyte solutions, J. Membr. Sci., 267 (2005) 50–57.
[43] A. Ślęzak, S. Grzegorczyn, J. Jasik-Ślęzak, K. Michalska-Małecka, Natural convection as an asymmetrical factor of the transport through porous membrane, Transp. Porous Media, 84 (2010) 685–698.
[44] K. Dworecki, A. Ślęzak, B. Ornal-Wąsik, S. Wąsik, Effect of hydrodynamic instabilities on solute transport in a membrane system, J. Membr. Sci., 265 (2005) 94–100.
[45] J.S. Jasik-Ślęzak, K.M. Olszówka, A. Ślęzak, Estimation of thickness of concentration boundary layers by osmotic volume flux determination, Gen. Physiol. Biophys., 30 (2011) 186–195.
[46] A. Ślęzak, Irreversible thermodynamic model equations of the transport across a horizontally mounted membrane, Biophys. Chem., 34 (1989) 91–102.
[47] A. Ślęzak, K. Dworecki, J. Jasik-Ślęzak, J. Wąsik, Method to determine the critical concentration Rayleigh number in isothermal passive membrane transport processes, Desalination, 168 (2004) 397–412.
[48] A. Ślęzak, K. Dworecki, J.E. Anderson, Gravitational effects on transmembrane flux: the Rayleigh—Taylor convective instability, J. Membr. Sci., 23 (1985) 71–81.
[49] H. Klinkman, M. Holtz, W. Wilgerodt, G. Wilke, D. Schoenfelder, Nephrophan–Eine neue dialysemembranen, Z. Urol. Nephrol., 62 (1969) 285–292.
[50] T. Richter, S. Keipert, In vitro permeation studies comparing bovine nasal mucosa, porcine cornea and artificial membrane:

androstenedione in microemulsions and their components, Eur. J. Pharm. Biopharm., 58 (2004) 137–143.
[51] Th. F. Vandamme, Microemulsions as ocular drug delivery systems: recent developments and future challenges, Prog. Retin. Eye Res., 21 (2002) 15–34.
[52] O. Kedem, S.R. Caplan, Degree of coupling and its relation to efficiency of energy conversion, Trans. Faraday Soc., 61 (1965) 1897–1911.
[53] S. Bason, O. Kedem, V. Freger, Determination of concentration-dependent transport coefficients in nanofiltration: experimental evaluation of coefficients, J. Membr. Sci., 310 (2008) 326–204.
[54] I. Ślęzak-Prochazka, K.M. Batko, A. Ślęzak, evaluation of transport properties and energy conversion of bacterial cellulose membrane using Peusner network thermodynamics, Entropy, 25 (2023) 3, doi: 10.3390/e25010003.
[55] K. Dworecki, Interferometric investigation of near-membrane diffusion layers, J. Biol. Phys., 21 (1995) 37–49.
[56] K. Dworecki, S. Wąsik, A. Ślęzak, Temporal and spatial structure of the concentration boundary layers in a membrane system, Physica A, 326 (2003) 360–369.
[57] K. Dworecki, A. Ślęzak, M. Drabik, B. Ornal-Wąsik, S. Wąsik, Determination of the membrane permeability coefficient under concentration polarisation conditions, Desalination, 198 (2006) 326–334.